



POLYTECHNIC OF BARI

DEPARTMENT OF ELECTRICAL AND INFORMATION ENGINEERING

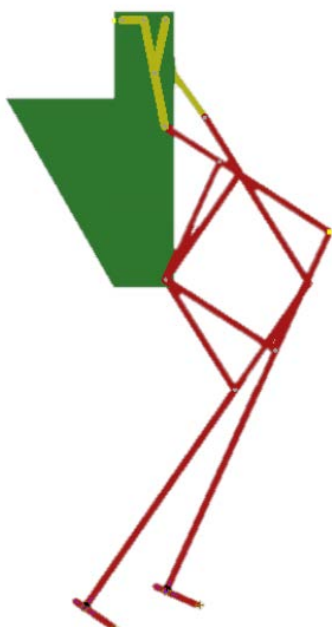
AUTOMATION ENGINEERING MASTER'S DEGREE

---

Course on APPLIED MECHANICS - FUNCTIONAL DESIGN

Prof. Engr. Mario Massimo **FOGLIA**

*Project work:*  
**TWO-LEGGED WALKING ROBOT**



*Students:*  
**D'ALESSANDRO** Vito Ivano  
**VENEZIA** Antonio

---

ACADEMIC YEAR 2019-2020



### Abstract

The aim of this project is the analysis on the sagittal plane of a two legged walking robot, with a reduced number of DOF (Degrees Of Freedom). More in depth, kinematics and dynamics model are proposed in order to find different solution to issues that afflict this type of machines, such as high number of actuators and, consequently, high power consumption. Using a combination of basic linkages such as Hoeken linkage and pantograph, a 1 DOF single leg is obtained. Two solution are studied to avoid instability during the walking of the robot, in particular by using a parallel extension and a torsion spring placed in the ankle joint. Each model have been implemented and verified using MATLAB environment and reproduced in Autodesk Inventor PRO 2020, and different simulations have been provided.



## Contents

|                        |   |           |
|------------------------|---|-----------|
| <b>1</b>               | <b>Introduction</b>                                     | <b>4</b>  |
| <b>2</b>               | <b>State of the Art</b>                                 | <b>5</b>  |
| <b>3</b>               | <b>Geometric Analysis</b>                               | <b>11</b> |
| 3.1                    | Hoeken straight-line linkage . . . . .                  | 11        |
| 3.2                    | Pantograph . . . . .                                    | 12        |
| 3.3                    | Single Leg Mechanism . . . . .                          | 13        |
| 3.4                    | Degrees of Freedom without Parallel Extension . . . . . | 14        |
| 3.5                    | Parallel Extension . . . . .                            | 15        |
| 3.6                    | Single Leg Mechanism with Parallel Extension . . . . .  | 16        |
| 3.7                    | Degrees of Freedom with Parallel Extension . . . . .    | 17        |
| <b>4</b>               | <b>Forward Kinematics</b>                               | <b>18</b> |
| 4.1                    | Homogeneous Transformation Matrices . . . . .           | 18        |
| 4.2                    | Analysis Without Parallel Extension . . . . .           | 19        |
| 4.2.1                  | Closed Loop Equations . . . . .                         | 21        |
| 4.2.2                  | Simulation and Results . . . . .                        | 23        |
| 4.2.3                  | Body Posture Analysis In Walking Phase . . . . .        | 27        |
| 4.3                    | Analysis with Parallel Extension . . . . .              | 30        |
| 4.3.1                  | Closed Loop Equations . . . . .                         | 31        |
| 4.3.2                  | Simulation and Results . . . . .                        | 33        |
| 4.3.3                  | Body Posture Analysis In Walking Phase . . . . .        | 33        |
| 4.3.4                  | Simulations and Results . . . . .                       | 33        |
| <b>5</b>               | <b>Differential Kinematics</b>                          | <b>35</b> |
| <b>6</b>               | <b>Autodesk Inventor Professional 2020</b>              | <b>37</b> |
| 6.1                    | Prototype of Walking Robot . . . . .                    | 37        |
| 6.2                    | Path of Ankle and Toe . . . . .                         | 37        |
| 6.3                    | Linear Velocity and Acceleration of the Ankle . . . . . | 38        |
| <b>7</b>               | <b>Inverse Dynamics</b>                                 | <b>40</b> |
| 7.1                    | Mass Distribution . . . . .                             | 40        |
| 7.2                    | Torsion Spring . . . . .                                | 42        |
| 7.3                    | Quasi-Static . . . . .                                  | 42        |
| 7.3.1                  | Equation of Motion . . . . .                            | 42        |
| 7.3.2                  | Simulation and Results . . . . .                        | 44        |
| 7.4                    | Dynamic Analysis . . . . .                              | 45        |
| 7.4.1                  | Equation of motion . . . . .                            | 45        |
| 7.4.2                  | Simulation and Results - First Simulation . . . . .     | 46        |
| 7.4.3                  | Simulation and Results - Second Simulation . . . . .    | 47        |
| 7.4.4                  | Simulation and Results - Third Simulation . . . . .     | 48        |
| 7.4.5                  | Simulation and Results - Fourth Simulation . . . . .    | 49        |
| <b>8</b>               | <b>Conclusions &amp; Future Works</b>                   | <b>50</b> |
| <b>References</b>      |   | <b>51</b> |
| <b>List of Figures</b> |   | <b>52</b> |



**List of Tables**

**53**



## 1 Introduction

A humanoid robot is a robot based on the appearance of a human body. Humanoid walking robot is a very challenging field of research due to the complexity of synthesizing stable walking gaits for these systems. Despite of the great advances performed until now in the field of the biped robots, there is still a lot to do. The major disadvantages walking robots present are related to the weight and the power consumption due to a high number of actuators that are used to control the high degrees of freedom (DOF) they have. Because of the high power consumption, in the majority of cases this technology shouldn't be suitable for many tasks and/or environments: infact, in most of cases around 30% of the total weight is related to the actuators and wires, and more than 25% to the reduction systems [1]. The study in new mechanisms and kinematics chains let us to obtain new designs of walking robots supporting movements of the most known humanoids but reducing the number of degrees of freedom (minor number of actuators). Therefore, it is possible to reduce the weight and energetic consumption drastically and, consequently, the cost of the robot. In order to achieve these results, the gait pattern on the sagittal plane of a two legged walking robot with 1 DOF for each leg has been studied, in which the leg mechanism is the combination of a Hoeken straight-line linkage (also known as lambda mechanism because of the figure it represents) and pantograph mechanism that is a transmission mechanism that scale a particular figure. This kind of leg mechanism has 1 DOF achieving the minimization of the number of actuators to obtain a feasible gait pattern.

Due to instability on the sagittal plane, two different solutions have been analyzed:

- a parallel extension for each leg;
- a torsion spring placed on the ankle joint for each leg.



## 2 State of the Art

Through history, engineers and inventors tried to imitate the human walking patterns in order to develop robot able to walk or even run dealing with different type of environments. A typical walk consists of a repeated gait cycle. The cycle itself contains two phases [2]:

- stance phase
- swing phase

The stance phase, accounts for 60% of the gait cycle and can be divided into three other phases:

- heel strike phase, in which the foot hits the ground heel first;
- support phase, in which the rest of the leading foot hits the ground, and the muscles work to cope with the force passing through the leg;
- toe-off phase, in which the foot prepares to leave the ground (heel first,toes last).

The swing phase occurs when one foot is on the ground and one in the air. The foot that is in the air is said to be in the “Swing” phase of gait. It can be divided in other two phases:

- leg lift, in which the lower limb is raised in preparation for the swing stage after foot has left the ground;
- swing phase, when the raised leg is propelled forward.

All these phases are shown in Fig. 2.1.

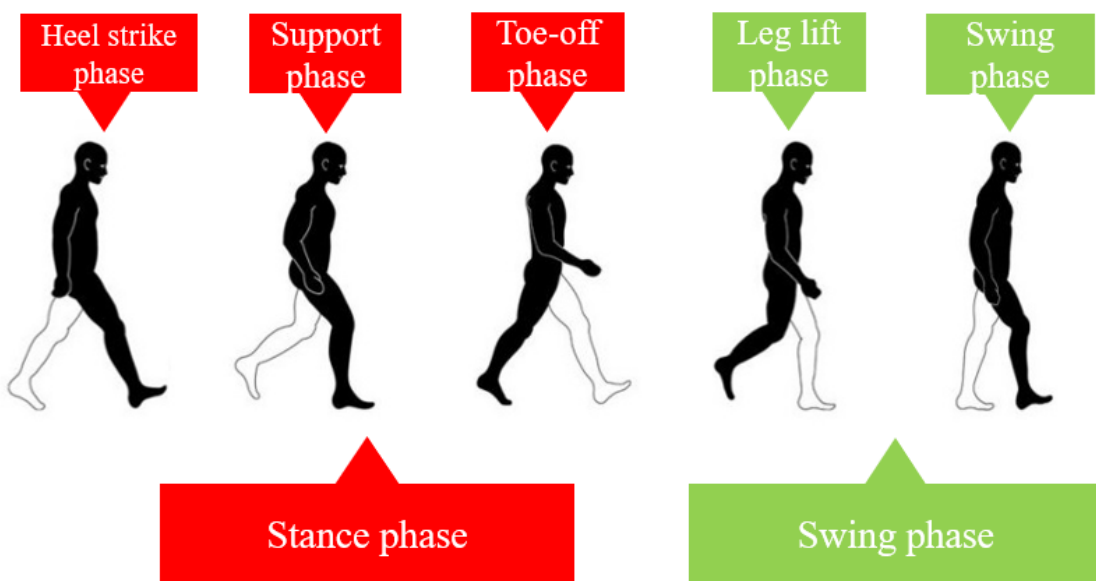


Figure 2.1: Walking phases

The first walking robots were used for entertainment. The first ideas about implementing legged locomotion vehicles date from the fifteenth century [3]. Between 1495 and 1497 Leonardo da Vinci designed and possibly built the first articulated anthropomorphic robot in the history of western



civilization that probably could be used to animate parties at the Sforza court in Milan. In the notes rediscovered in the 1950s in the *Atlantic Codex* and in small pocket notebooks dating from around 1495-1497, there are detailed drawings for a mechanical knight : according to Rosheim's studies this armoured knight was designed to sit up, wave its arms and move its head via a flexible neck while opening and closing its anatomically correct jaw. Leonardo's robot outwardly appears as a typical German-Italian suit of armour of the late fifteenth century. It was made of wood with parts of leather and brass or bronze and was cable operated. The robot project was a significant outgrowth of Leonardo's anatomical and kinesiology studies, forming a bridge between his mechanical work and his anatomical studies (Rosheim, 1997).

The mechanical design of Leonardo's invention is shown in Fig. 2.2.



Figure 2.2: Mechanical knight of Leonardo da Vinci

In 1878 the Russian mathematician Chebyshev presented a model for a locomotion system at the World Fair in Paris shown in Fig. 2.3. The mechanism consists of four identical Chebyshev lambda-shaped parallel motions:  $C'A_1B_1C$ ,  $C'A_2B_2C$ ,  $C'_1A_3B_3C_1$  and  $C_1A_4B_4C_1$ . Together with cranks 7 and 8, links 5 and 6 form parallel-crank linkage  $A_1A_2A_4A_3$ . If frame 9 is fixed, then points  $M_1, M_2, M_3$  and  $M_4$  describe connecting-rod curves of a shape resembling curve a-a' and having an approximately straight portion b-b' which corresponds to rotation of cranks 7 and 8 through an angle of 180 degree. Secured rigidly to link 10 are "feet" 1 and 4, and to link 11 are "feet" 2 and 3. If frame 9 is moved in rectilinear translation from the position shown in the drawing in either direction, then, while points  $M_1$  and  $M_4$  remain on their straight portions of their relative paths, "feet" 1 and 4 are stationary and "feet" 2 and 3 move along the direction of motion of frame 9. At the moment that points  $M_1$  and  $M_4$  leave the straight portion of their paths, points  $M_2$  and  $M_3$  begin the straight portion of their paths. At this, "feet" 2 and 3 will be stationary and "feet" 1 and 4 will move along the direction of motion of frame 9. Thus the mechanism seems to reproduce the motions of the legs of an animal.

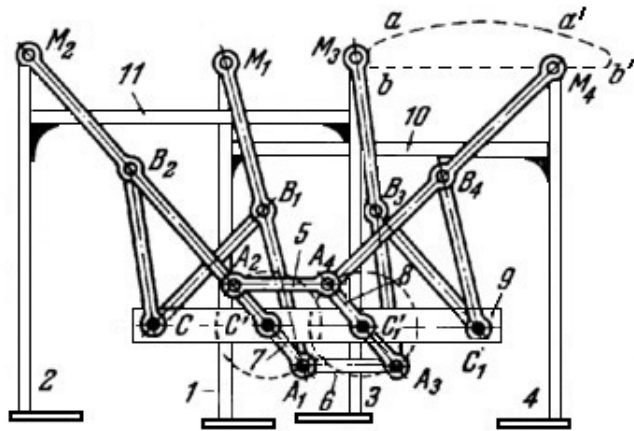


Figure 2.3: Chebyshev multiple-bar walking mechanism

The research in biped locomotion, when compared with the multilegged case, has advanced slower due to the difficulty in establishing a stable control because biped robots are more demanding regarding its dynamic balance.

In 1969 Ichiro Kato developed the first biped robot able to walk called WAP-1 at the Humanoid Research Laboratory. For its actuation, this robot had artificial rubber muscles, pneumatically actuated, and the biped locomotion was achieved through the playback of previously taught movements. The main initial limitation of this machine was its low speed, needing 90 seconds in order to complete a step. Latter advancements allowed reaching speeds near those achieved by the human being. The WAP-1 robot is shown in the Fig. 2.4.

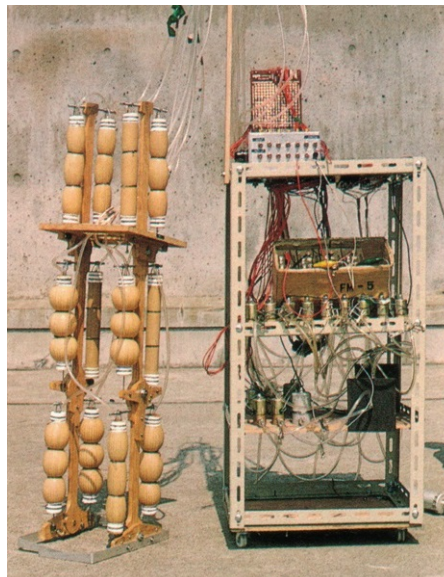


Figure 2.4: WAP-1 walking robot



Kato continued in the research and in 1970 he developed WAP-2. A movement of WAP-2 was significantly faster than movement of WAP-1. Moreover, in 1971 Kato developed WAP-3 which was able to move in the three-dimensional way as the first biped in the world at all. It was able to move its center of gravity on the frontal plane so that it was able to not only walk on a flat surface but also descend and ascend a staircase or slope and turn while walking.

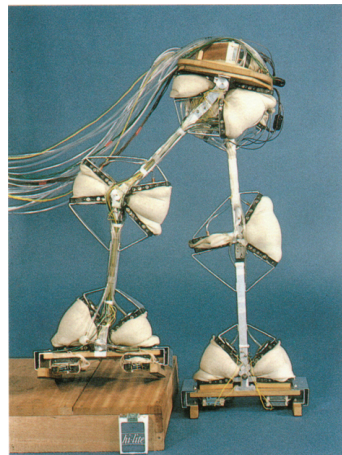


Figure 2.5: WAP-3 walking robot

In the beginning of the 1980's, Kato and his co-workers built the biped WL-9DR that walked with a quasi-dynamic gait. This machine presented ten hydraulic actuated DOF and two relatively large feet, as shown in Fig.2.6. This system adopted a static locomotion mode, moving along a pre-planned trajectory, in order to keep the centre of gravity inside the support base supplied by the support foot. However, once on each locomotion cycle, the machine temporary unbalanced itself (leaning forward) in order to rapidly transfer support from one foot to the other. Before the end of the transfer, the front foot positioned itself in order to make the machine passively return to equilibrium, without needing active control. In 1984 this machine was controlled through a quasi-dynamic gait, taking around one minute to perform a dozen 0.5 m steps.

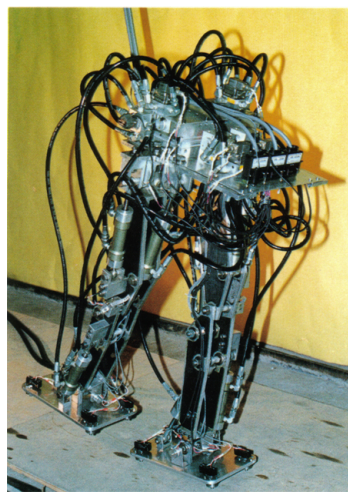


Figure 2.6: WL-9DR walking robot



Nowadays there is a large variety of biped robots presenting humanoid shape and having good locomotion capabilities. One of the biped robots presenting better locomotion capabilities is the Honda Humanoid Robot (Fig.2.7). This robot project began in 1986 and the key ideas adopted for its development were “intelligence” and “mobility”, since the robot should coexist and cooperate with human beings. The development of the Honda Humanoid Robot was based on data retrieved from human locomotion.

Honda’s idea was to create a robot that could be used in dairy life, in opposition of a robot developed for a particular application, aiming its introduction in factories. Honda also specified three functions that had to be fulfilled: the locomotion speed should correspond to that of a human being (approximately  $3 \text{ km/h}$ ), the robot structure should be prepared to support arms with hand and should be able to climb up and down stairs. The latest version of this robot, so called ASIMO (Advanced Step in Innovative MObility) model, was concluded in 2000, having 1.2 m height and a 43 kg weight. The ASIMO has 26 DOF (Degrees of Freedom), electrically actuated, and can hold 0.5 kg on each hand. It is a completely autonomous robot, either in terms of processing capability, either in terms of power (it transports on its back batteries that allow 15 minutes autonomy).



Figure 2.7: P3 model on the left and ASIMO on the right

The huge increment that has been verified in the research on biped locomotion in the last years is partially due to the implementation in Japan of the HRP – Humanoid Robotics Program. One of the examples of biped robots that have been developed under this program is the HRP-2 humanoid (Fig.2.8). This robot is able to move on irregular surfaces, at  $2/3$  of the normal human speed, and it is able to cross narrow passages, modifying its gait for that purpose. In case the robot loses balance and falls, besides the fall being controlled in order to minimize eventual damages on the structure, it is still capable of rise alone.



Figure 2.8: HPR-2 humanoid robot



All these kind of humanoid robot have a several number of actuators that are used to control the high degrees of freedom they have, corresponding to higher power consumption. For this reason in the last years, different research groups have developed robots based on passive walking techniques. An example of this kind of robot is the prototype designed and built at the Laboratory of Robotics and Mechatronics in Cassino [4]: in Fig.2.9 a prototype of a single DOF biped robot fixed on a supporting test bed is shown. It consists of two leg mechanisms with a Chebyshev-Pantograph linkage architecture. The leg mechanisms are connected to the body with revolute joints and they are actuated by only one DC motor through a gear box. The actuated crank angles of the two leg mechanisms are 180 degrees synchronized. Therefore, when one leg mechanism is in non-propelling phase another leg mechanism is in propelling phase and vice versa.

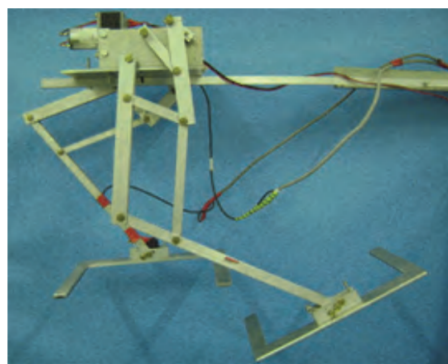


Figure 2.9: A prototype of a single DOF biped robot at LARM

The main problem of this two-legged walking robot is the instability during the walking and, for this reason, another kind of 1 DOF walking robot at the Polithecnic of Valencia, called Pasibot has been prototyped [1]. The main difference is the presence of a parallel extension, a four bar-linkage that provides a trunk trajectory purely translatory on the sagittal plane. The pasibot robot is shown in Fig.2.10.

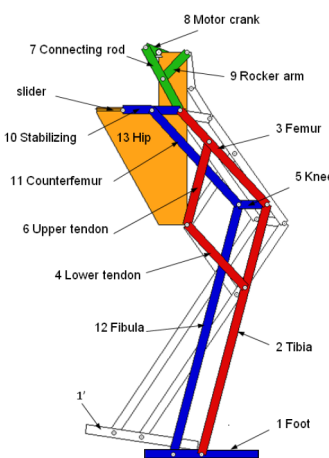


Figure 2.10: Pasibot Robot



### 3 Geometric Analysis

In this study a prototype of walking robot called 'Pasibot' has been analyzed. In order to define a kinematics and dynamics model of the walking robot, a geometric analysis of the three main mechanisms is mandatory. In the following sections, the Hoeken straight-line linkage, the pantograph and the parallel extension mechanisms- are presented. It's important to underline that length of each link of the mechanism are defined in [5].

#### 3.1 Hoeken straight-line linkage

The Hoeken linkage is a four-bar mechanism that converts rotational motion to approximate straight-line motion. The linkage was first published in 1926 and is considered as a cognate of Chebyshev linkage having a very nearly constant velocity along the center portion of its straight-line motion [6].

Length of links of the Hoeken's straight-line linkage are shown in Tab.3.1.1, where links are expressed in function of crank's length  $L$ . Notice that link's length  $L_0$  depends on a constant  $K$  that allows to change the trajectory of the end effector <sup>4</sup><sup>1</sup>.

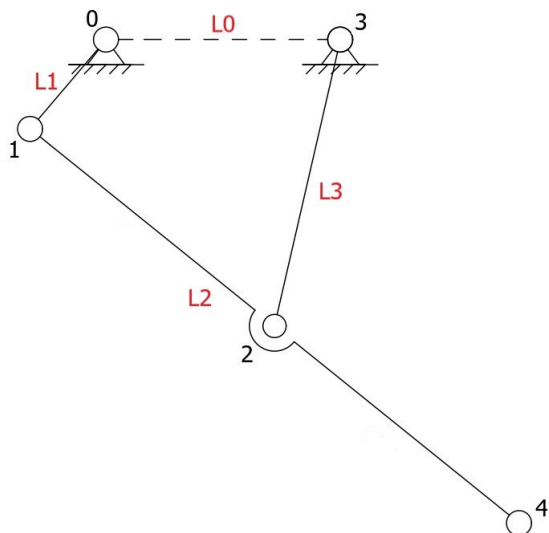


Figure 3.1.1: Hoeken straight-line linkage

| Link  | Length |
|-------|--------|
| $L_0$ | $KL$   |
| $L_1$ | $L$    |
| $L_2$ | $5L$   |
| $L_3$ | $2.5L$ |

Table 3.1.1: Length of Hoeken's links

<sup>1</sup>The link ratios of Hoeken straight-line linkage have been reported differently by various authors. In the study case, the ratios used are those first reported.



### 3.2 Pantograph

The pantograph (Greek: "all-writer") is a four-bar mechanism used to scale shapes followed by a particular joint. Its basis is a parallelogram of four links connected by revolute joints 5-6-7-8, as shown in Fig. 3.2.1. Considering similar triangles (4 - 5 - 8 and 8 - 7 - 13), it can be demonstrate that the ratio with which the mechanism scale a particular figure followed by joint 4 in the study case is:

$$k = \frac{b}{a} = 2 \quad (1)$$

Length of links of the pantograph are shown in Tab.3.2.1, where links are expressed in function of  $L$ .

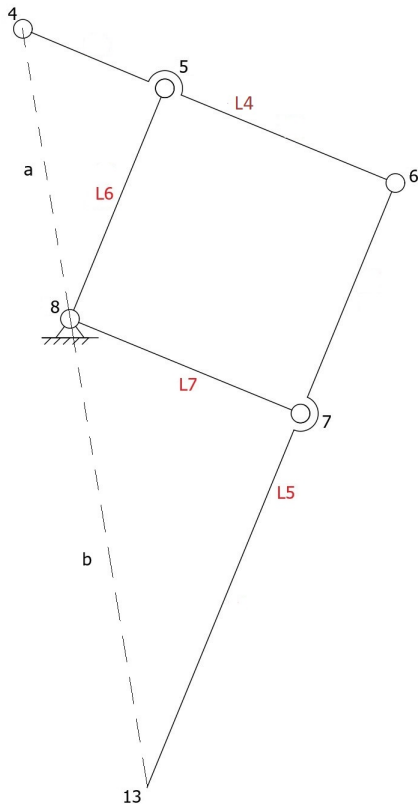


Figure 3.2.1: Pantograph

| Link | Length |
|------|--------|
| L4   | 9L     |
| L5   | 18L    |
| L6   | 6L     |
| L7   | 6L     |

Table 3.2.1: Length of pantograph's links



### 3.3 Single Leg Mechanism

In Fig.3.3.1 a complete single leg mechanism of the walking robot is shown, deriving by the combination of the Hoeken linkage and pantograph, while Tab.3.3.1 shows length of each link. Foot hasn't been considered yet, and it will be taken into account in the following sections.

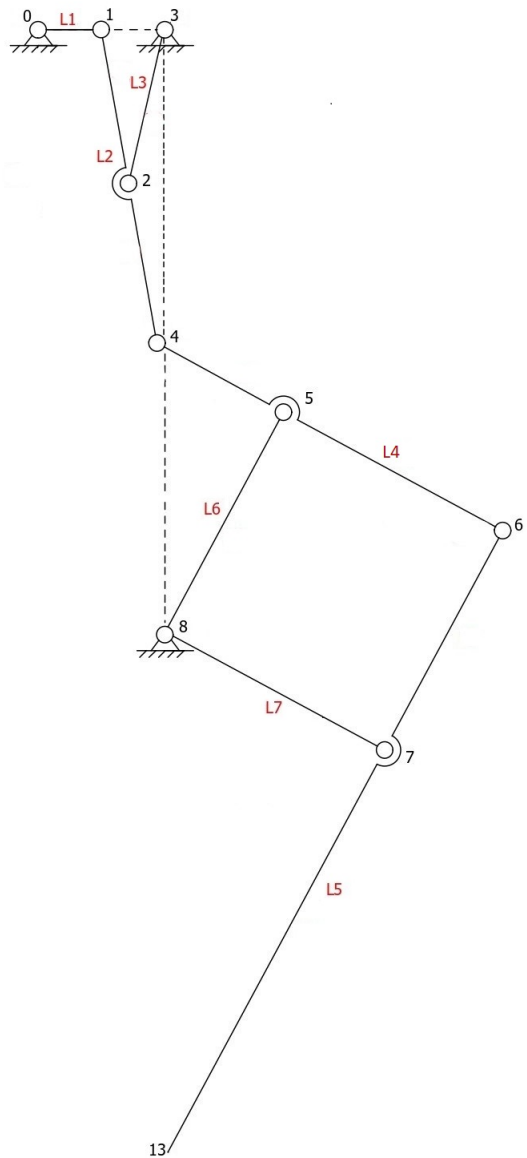


Figure 3.3.1: Single leg mechanism



| Link | Length |
|------|--------|
| L0   | KL     |
| L1   | L      |
| L2   | 5L     |
| L3   | 2.5L   |
| L4   | 9L     |
| L5   | 18L    |
| L6   | 6L     |
| L7   | 6L     |

Table 3.3.1: Length of Links

### 3.4 Degrees of Freedom without Parallel Extension

The Grubler formula allows to find the number of degrees of freedom of a mechanism using the following equation:

$$DOF = d \cdot (m - 1) - 2 \cdot C_1 - C_2 \quad (2)$$

where

- $d$  is the dimension of the motion space of all members of the mechanism;
- $m$  is the number of rigid bodies in the mechanical system considered;
- $C_1$  is the number of lower pairs (such as revolute and prismatic pairs);
- $C_2$  is the number of higher pairs (such as cam).

In the study case, the previous parameters for the single leg mechanism shown in Fig.3.3.1 are:

- $d = 3$ , because the mechanism is planar;
- $m = 8$ , because the number of links including the chassis is equal to 8;
- $C_1 = 10$ , because there are 9 lower pairs (that is one degree of freedom kinematic pair), where the one in joint 8 must be considered twice;
- $C_2 = 0$ , because there aren't higher pairs in the mechanism.

Substituting these parameters in Eq.2, the degrees of freedom of the single leg mechanism without parallel extension are:

$$DOF = 3 \cdot (8 - 1) - 2 \cdot 10 - 0 = 21 - 20 = 1$$

### 3.5 Parallel Extension

In order to improve stability of the walking robot on the sagittal plane during the walking phases, a stabilization system has been considered as can be seen in Fig.3.5.1, comprising a set of links that run parallel to the two longest links of the pantograph, which ensures the stabilizer link  $L_8$  and the foot of the biped remain parallel, avoiding a non-perfect contact between foot and ground [7]. The stabilizer link determines the orientation of the foot while attached to the connecting rod of the Hoeken straight-line linkage  $L_2$ , and freely to slide on a prismatic joint 10 placed on the hip . This mechanism keeps the swing leg's foot at a certain bias while in flight and retain a horizontal position of the standing leg's foot during the walking. Length of parallel extension's links are shown in Tab.3.5.1, expressed in function of  $L$ .

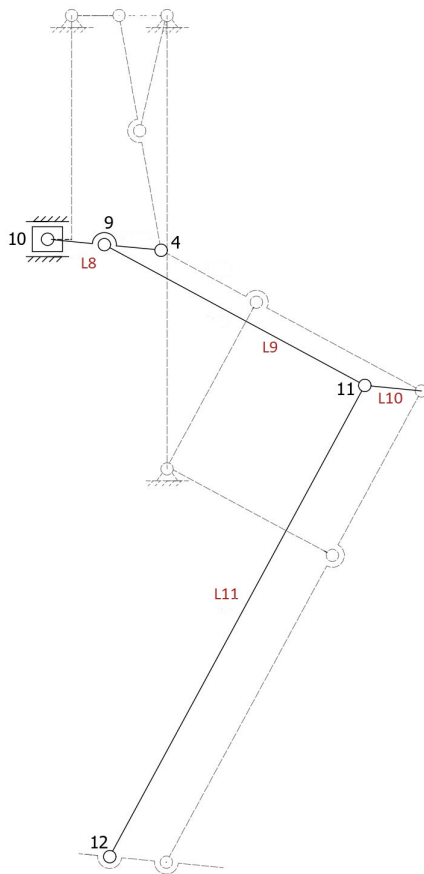


Figure 3.5.1: Parallel Extension

| Link     | Length |
|----------|--------|
| $L_8$    | $4.2L$ |
| $L_9$    | $9L$   |
| $L_{10}$ | $2.1L$ |
| $L_{11}$ | $18L$  |

Table 3.5.1: Length of links Parallel Extension

### 3.6 Single Leg Mechanism with Parallel Extension

In Fig.3.6.1 a complete single leg mechanism is proposed, including the parallel extension and Tab.3.6.1 shows length of each link.

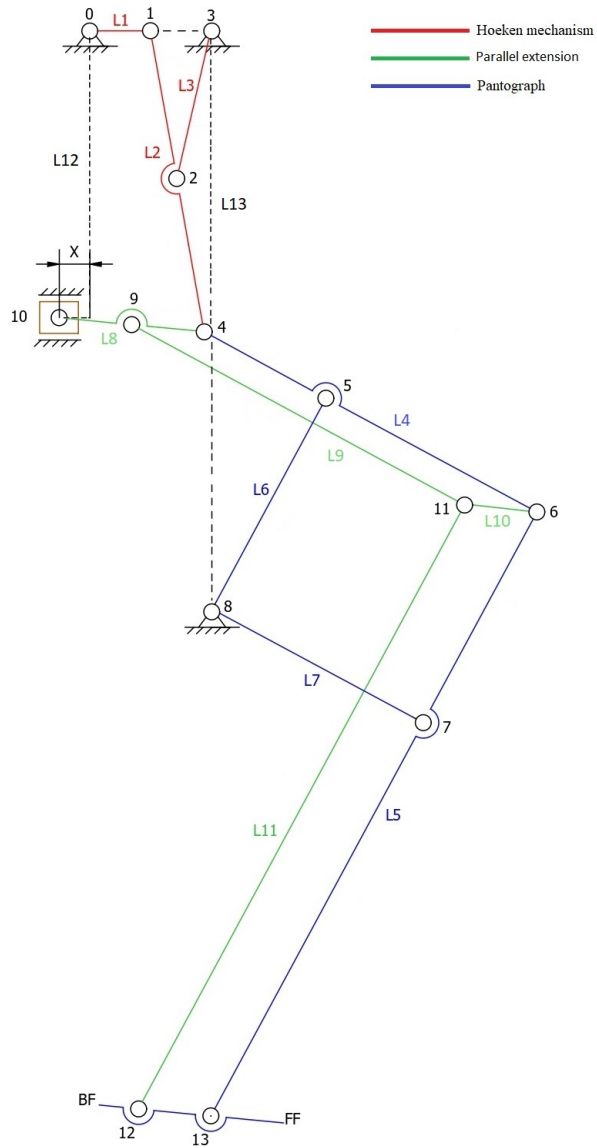


Figure 3.6.1: Single leg with parallel extension



| Link | Length |
|------|--------|
| L0   | KL     |
| L1   | L      |
| L2   | 5L     |
| L3   | 2.5L   |
| L4   | 9L     |
| L5   | 18L    |
| L6   | 6L     |
| L7   | 6L     |
| L8   | 4.2L   |
| L9   | 9L     |
| L10  | 2.1L   |
| L11  | 18L    |
| L12  | 4L     |
| L13  | 12L    |

Table 3.6.1: Length of Links

The length of each link of the mechanism is assumed to be known and refers to [5].

### 3.7 Degrees of Freedom with Parallel Extension

Grubler formula parameters for the single leg mechanism with parallel extension are:

- $d = 3$ , because it has been considered a planar mechanism;
- $m = 12$ , because the number of rigid bodies is equal to 12;
- $C_1 = 16$ , because there are 15 lower pairs (that is one degree of freedom kinematic pair) where the one in joint 8 must be considered twice;
- $C_2 = 0$ , because there aren't higher pairs in the mechanism considered.

Substituting them in Eq.2, the degrees of freedom of the mechanism are:

$$DOF = 3 \cdot (12 - 1) - 2 \cdot 16 - 0 = 33 - 32 = 1$$

## 4 Forward Kinematics

Forward kinematics allows to determine the pose of the end-effector as a function of the joint variables of the mechanism considered. In a first analysis, foot corresponds to the end effector and its position and orientation depends on the angular position  $\theta_1$  of the crank  $L1$  (corresponding to the only actuated joint). Then, the body posture analysis in the walking phases (Fig.2.1) is presented. In the following sections, two mechanical system for the walking robot have been proposed, as shown in Fig.4.1. More in depth, a parallel extension has been considered in addition to the Hoeken straight-line linkage and pantograph, in order to prevent instability on the sagittal plane.

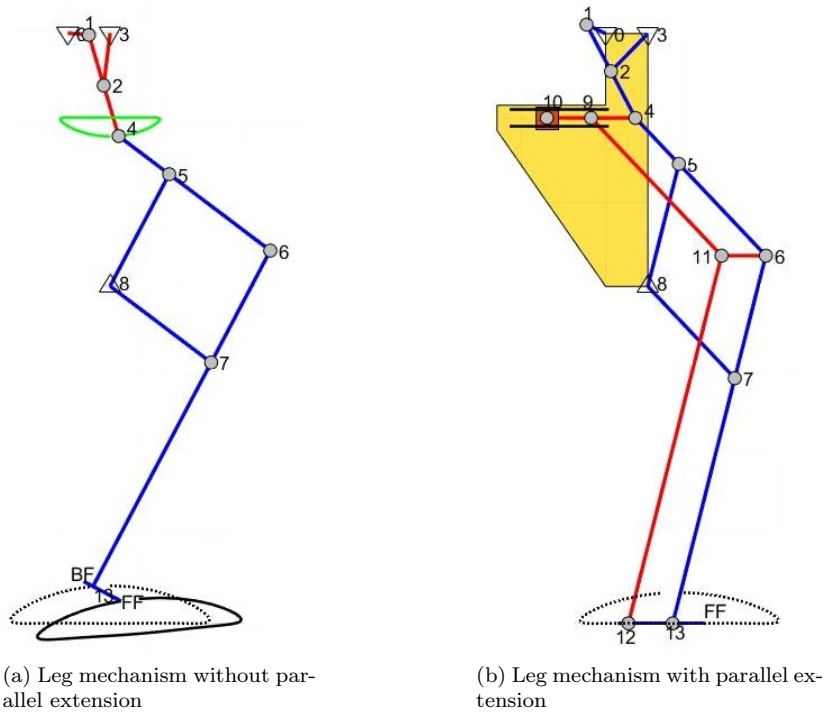


Figure 4.1: Single leg mechanism

### 4.1 Homogeneous Transformation Matrices

In order to analyze joints' position, a set of transformation matrices can be defined, where  $T_i^{i-1}$  is a transformation matrix that expresses the coordinate transformation from frame  $i$  to  $i - 1$ .

If the Denavit-Hartenberg convention is considered, this transformation matrix depends on four different parameters and is defined as follows:

$$T_i^{i-1} = \begin{bmatrix} \cos(\theta_i) & -\sin(\theta_i)\cos(\alpha_i) & \sin(\theta_i)\sin(\alpha_i) & L_i\cos(\theta_i) \\ \sin(\theta_i) & \cos(\theta_i)\cos(\alpha_i) & -\cos(\theta_i)\sin(\alpha_i) & L_i\sin(\theta_i) \\ 0 & \sin(\alpha_i) & \cos(\alpha_i) & d_i \\ 0 & 0 & 0 & 1 \end{bmatrix} \quad (3)$$

where

- $a_i$  is the distance between  $O_i$  and  $O'_i$ ;



- $d_i$  is the coordinate of  $O_i'$  along  $z_{i-1}$ ;
- $\alpha_i$  is the angle between axes  $z_{i-1}$  and  $z_i$  about axis  $x_i$  to be taken positive when rotation is made counter-clockwise;
- $\theta_i$  is the angle between axes  $x_{i-1}$  and  $x_i$  about axis  $z_{i-1}$  to be taken positive when rotation is made counter-clockwise.

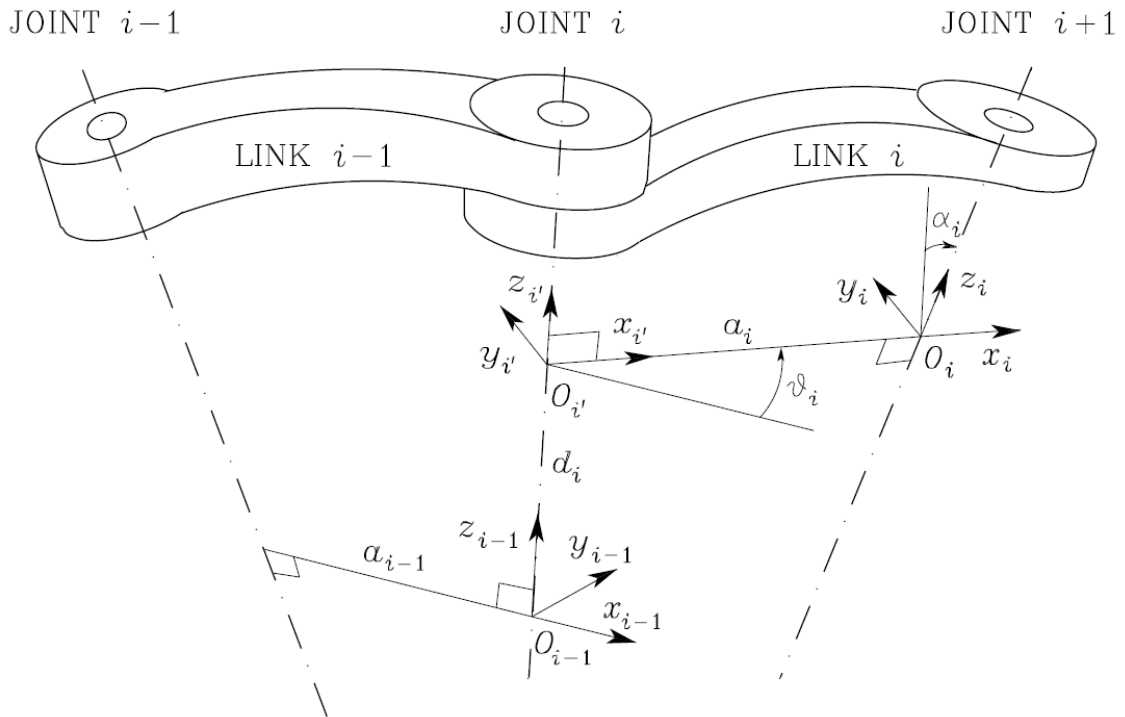


Figure 4.1.1: Denavit-Hartenberg kinematic parameters

## 4.2 Analysis Without Parallel Extension

Position and orientation of each link respect to a base frame can be computed by assigning a frame to each joint of the mechanism and determining the coordinate transformation between them, through homogeneous transformations, using the Denavit-Hartenberg convention, as in Fig.4.2.1 and Fig.4.2.2.

Because of the presence of closed loops, frames in cutted joints are highlighted with different colors.

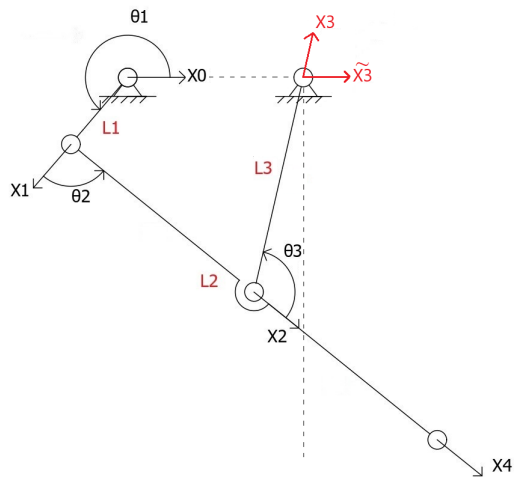


Figure 4.2.1: Frames' position and orientation Hoeken's Linkage

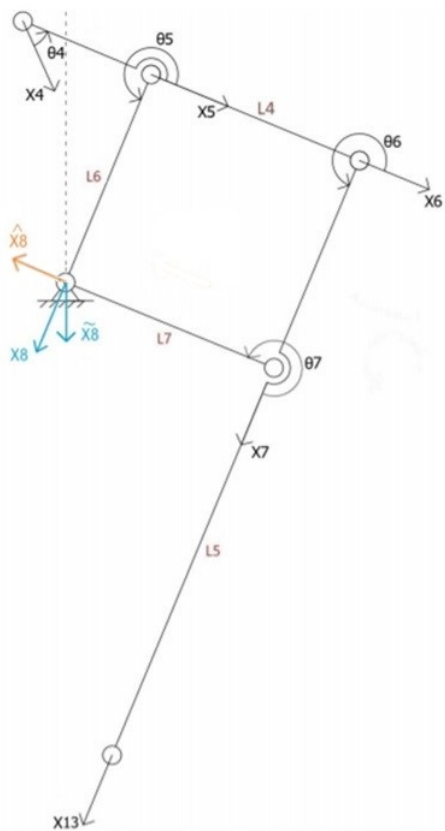


Figure 4.2.2: Frames' position and orientation pantograph



#### 4.2.1 Closed Loop Equations

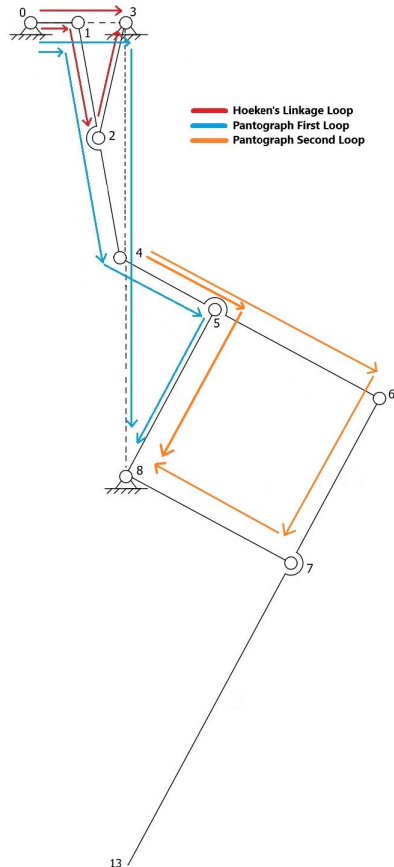


Figure 4.2.3: Closed Loops

As shown in Fig.4.2.3, three closed kinematic chains are taken into account. A closed chain can be virtually cut open at a joint to obtain an equivalent tree-structured open kinematic chain. After that, for each closed chain, a closed loop equation has to be determined and solved in order to compute joint variables. For these reasons, Denavit-Hartenberg table can be splitted into two sub-tables, one for each branch of the equivalent tree structure, as in Tab.4.2.1, Tab.4.2.2 and Tab.4.2.3.

| Frame | $a_i$ | $\alpha_i$ | $d_i$ | $\theta_i$ |
|-------|-------|------------|-------|------------|
| 1     | L1    | 0          | 0     | $\theta_1$ |
| 2     | L2/2  | 0          | 0     | $\theta_2$ |
| 3     | L3    | 0          | 0     | $\theta_3$ |

(a) Denavit-Hartenberg table for first branch (0-1-2-3)

| Frame       | $a_i$ | $\alpha_i$ | $d_i$ | $\theta_i$ |
|-------------|-------|------------|-------|------------|
| $\tilde{3}$ | L0    | 0          | 0     | 0          |

(b) Denavit-Hartenberg table for second branch (0- $\tilde{3}$ )

Table 4.2.1: First closed chain



| Frame | $a_i$ | $\alpha_i$ | $d_i$ | $\theta_i$ |
|-------|-------|------------|-------|------------|
| 1     | L1    | 0          | 0     | $\theta_1$ |
| 4     | L2    | 0          | 0     | $\theta_2$ |
| 5     | L4/3  | 0          | 0     | $\theta_4$ |
| 8     | L6    | 0          | 0     | $\theta_5$ |

(a) Denavit-Hartenberg table for first branch (0-1-4-5-8)

| Frame       | $a_i$ | $\alpha_i$ | $d_i$ | $\theta_i$ |
|-------------|-------|------------|-------|------------|
| $\tilde{3}$ | L0    | 0          | 0     | 0          |
| $\tilde{8}$ | L13   | 0          | 0     | $3\pi/2$   |

(b) Denavit-Hartenberg table for second branch (0- $\tilde{3}$ - $\tilde{8}$ )

Table 4.2.2: Second closed chain

| Frame | $a_i$ | $\alpha_i$ | $d_i$ | $\theta_i$ |
|-------|-------|------------|-------|------------|
| 1     | L1    | 0          | 0     | $\theta_1$ |
| 4     | L2    | 0          | 0     | $\theta_2$ |
| 5     | L4/3  | 0          | 0     | $\theta_4$ |
| 8     | L6    | 0          | 0     | $\theta_5$ |

(a) Denavit-Hartenberg table for first branch (0-1-4-5-8)

| Frame     | $a_i$ | $\alpha_i$ | $d_i$ | $\theta_i$ |
|-----------|-------|------------|-------|------------|
| 1         | L1    | 0          | 0     | $\theta_1$ |
| 4         | L2    | 0          | 0     | $\theta_2$ |
| 6         | L4    | 0          | 0     | $\theta_4$ |
| 7         | L5/3  | 0          | 0     | $\theta_6$ |
| $\hat{8}$ | L7    | 0          | 0     | $\theta_7$ |

(b) Denavit-Hartenberg table for second branch (0-1-4-6-7- $\hat{8}$ )

Table 4.2.3: Third closed chain

Using the Denavit-Hartenberg tables, transformation matrices can be easily determined:

$$\begin{aligned} T_2^0 &= T_1^0 T_2^1 \\ T_3^0 &= T_2^0 T_3^2 \\ T_4^0 &= T_2^0 T_4^2 \\ T_5^0 &= T_4^0 T_5^4 \\ T_6^0 &= T_5^0 T_6^5 \\ T_7^0 &= T_6^0 T_7^6 \\ T_8^0 &= T_5^0 T_8^5 \\ T_{\tilde{8}}^0 &= T_{\tilde{3}}^0 T_{\tilde{8}}^{\tilde{3}} \\ T_{\hat{8}}^0 &= T_7^0 T_{\hat{8}}^7 \\ T_{13}^0 &= T_7^0 T_{13}^7 \end{aligned}$$

After having defined all transformation matrices referred to base frame 0, closure equations for each loop have been defined.

For the first loop:

$$p_3^0(q_1') = p_3^0(q_1'') \quad (4)$$

where

$$q_1' = [\theta_1 \quad \theta_2 \quad \theta_3] \quad q_1'' = [0]$$



For the second one:

$$p_8^0(q_2') = p_8^0(q_2'') \quad (5)$$

where

$$q_2' = [\theta_1 \quad \theta_2 \quad \theta_4 \quad \theta_5] \quad q_2'' = [0 \quad 3\pi/2]$$

For the third one:

$$p_8^0(q_3') = p_8^0(q_3'') \quad (6)$$

where

$$q_3' = [\theta_1 \quad \theta_2 \quad \theta_4 \quad \theta_5] \quad q_3'' = [\theta_1 \quad \theta_2 \quad \theta_4 \quad \theta_6 \quad \theta_7]$$

#### 4.2.2 Simulation and Results

By solving Eq.4, Eq.5 and Eq.6, joint variables of the single leg mechanism can be determined. By varying  $L_0 = KL$ , that define distance between joint 0 and 3, different gait pattern can be obtained, as can be seen in Fig. 4.2.4. A feasible gait pattern is derived by setting

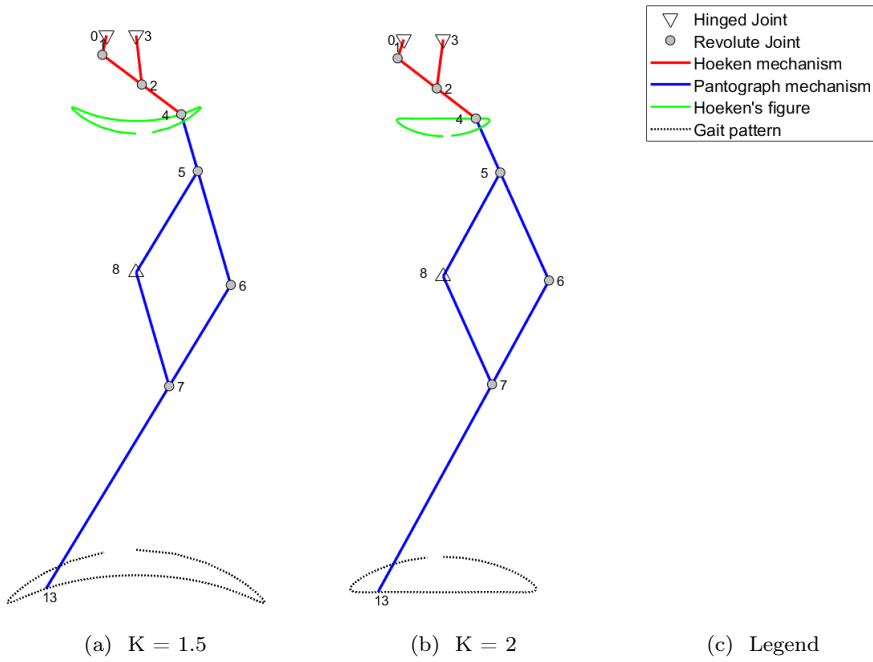


Figure 4.2.4: Comparison between two different gait pattern

$$K = 2$$

The step of the biped is characterized by a closed path, composed by two phases. The first phase has an almost straight-line path, which corresponds to the exact moment when the foot is in contact with the ground. The second phase (while the foot is in the air) has an almost elliptic path. This happens in each leg alternately, as they are geometrically identical, and their input cranks are around  $\pi$  radians out of phase with each other.



In order to compute forward kinematics for the second leg, an angular displacement of  $\pi$  should be considered for the actuated joint variable of the second leg  $\theta'_1$ .

Forward kinematics simulation of the walking robot is shown in Fig.4.2.5, where  $\theta_1$  and  $\theta'_1$  are the only actuated joint variables.

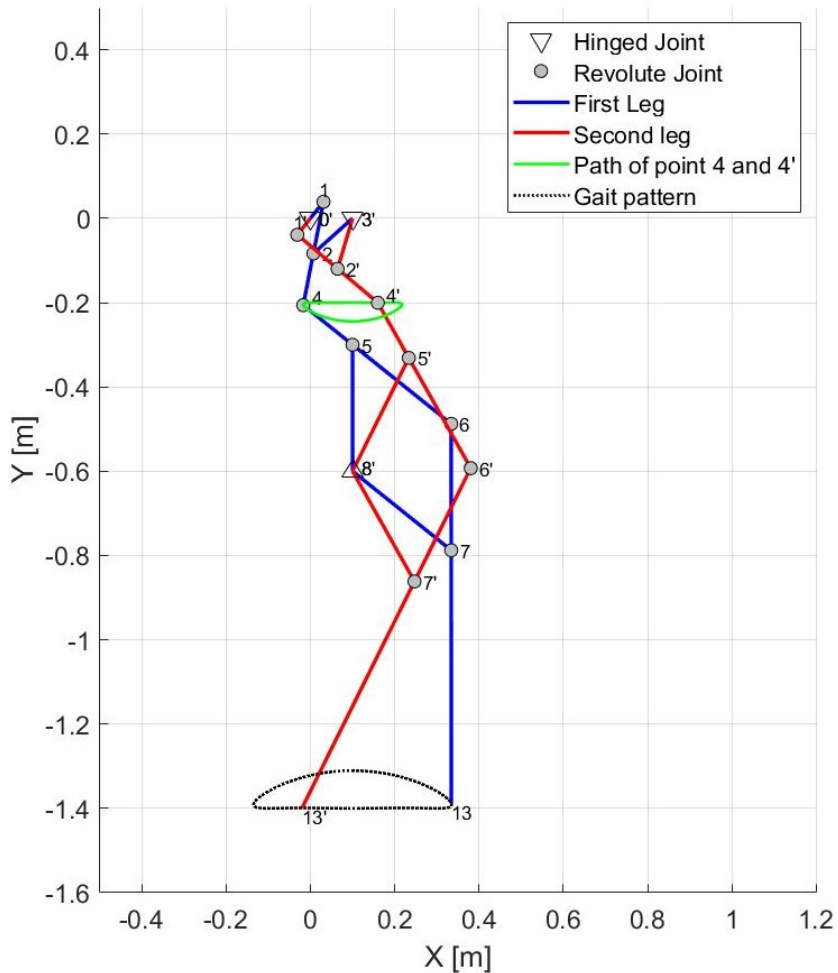


Figure 4.2.5: Gait pattern of two-legged walking robot

It's important to notice that in a first analysis,a punctiform foot has been considered. For a more realistic model of the walking robot, a foot with a fixed length rigidly connected to the tibia has been considered, so in this case the end effector will be the toe.

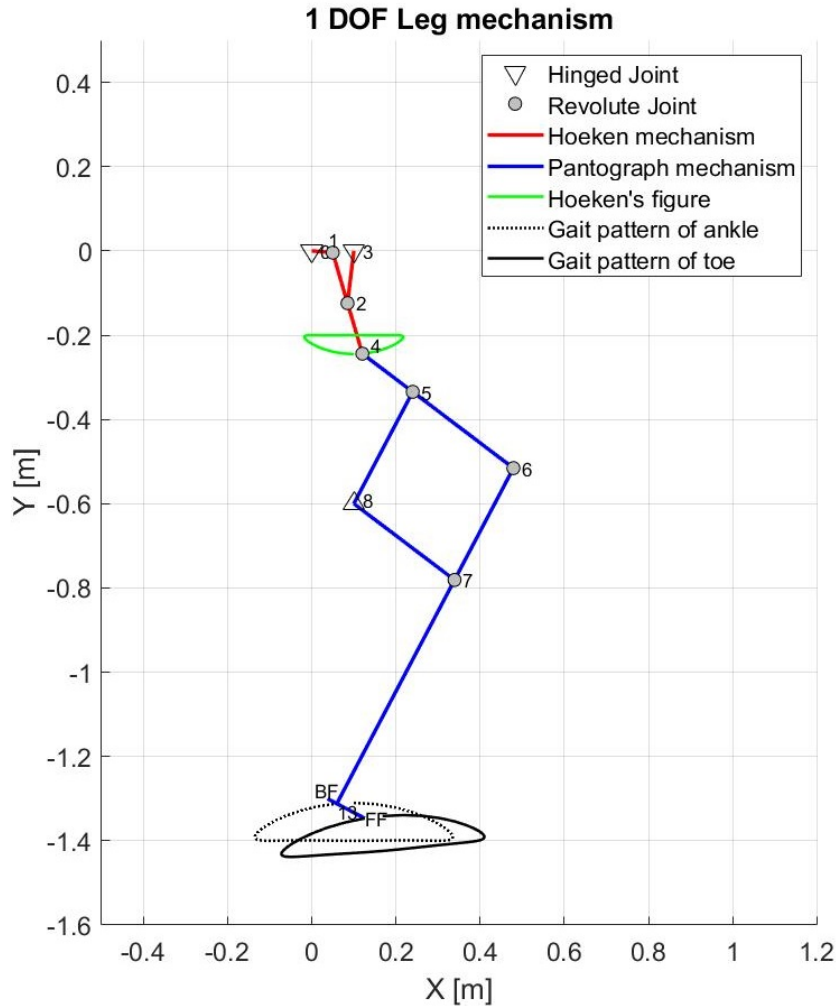


Figure 4.2.6: Gait pattern considering toe as end effector

Fig. 4.2.6 shows the gait pattern when a foot with a fixed length is considered: in particular, the distance between ankle and toe is set equal to  $1.5L$  whereas the distance between ankle and heel is equal to  $0.5L$ . In order to compute foot's position and orientation, two transformation matrices  $T_{FF}^0$  and  $T_{BF}^0$  have been defined: the first one is referred to the toe whereas the second one is referred to the heel. These two transformation matrices are defined following the Denavit-Hartenberg convention, shown in Tab.4.2.4.

As it can be seen, the ankle trajectory is quite different respect to the toe one: this because the foot, rigidly connected to the tibia, is considered perpendicular to the link  $L_5$ , so the toe will produce a trajectory comparables with the ankle trajectory, with a straight line portion non-parallel to the ground.

Due to that, foot couldn't get in contact with the ground with the plantar parallel to it which can cause instability of the walking robot during walking gait. For this reason, a parallel extension that provides to keep foot parallel to the ground during the straight-line portion should be considered.



| Frame | $a_i$ | $\alpha_i$ | $d_i$ | $\theta_i$ |
|-------|-------|------------|-------|------------|
| 1     | L1    | 0          | 0     | $\theta_1$ |
| 4     | L2    | 0          | 0     | $\theta_2$ |
| 6     | L4    | 0          | 0     | $\theta_4$ |
| 13    | L5    | 0          | 0     | $\theta_6$ |

| Frame | $a_i$ | $\alpha_i$ | $d_i$ | $\theta_i$ |
|-------|-------|------------|-------|------------|
| FF    | 1.5L  | 0          | 0     | $\pi/2$    |

(b) Denavit-Hartenberg table FF

| Frame | $a_i$ | $\alpha_i$ | $d_i$ | $\theta_i$ |
|-------|-------|------------|-------|------------|
| BF    | 0.5L  | 0          | 0     | $3\pi/2$   |

(c) Denavit-Hartenberg table BF

Table 4.2.4: Denavit-Hartenberg table with foot

As can be seen in Tab.4.2.4, two branches have been considered, allowing to define position and orientation of frames attached to toe and heel, respectively.



#### 4.2.3 Body Posture Analysis In Walking Phase

To analyze body posture, defining a world frame is mandatory. In this case a world frame with the origin coincident with the origin of the ankle joint's frame and x-axes parallel to the ground has been considered (Fig.4.2.7). Once have detected that frame, a transformation matrix  $T_0^{13}$  is defined, expressing position and orientation of frame 0, respect to the new base frame 13, attached to the ankle joint:

$$T_0^{13} = (T_{13}^0)^{-1}$$

Now it is necessary to define the transformation matrix  $T_{13}^W$  that define position and orientation of frame 13 respect to the world frame  $W$ . Because of the origin of world frame is coincident with the ankle joint's frame one,  $T_{13}^W$  only depends on the rotation angle  $\alpha$  around  $z-axis$ , between the two frames. In order to compute  $\alpha$ , it is necessary to extract from the transformation matrix  $T_{13}^0$  the rotation matrix  $R_{13}^0$ .

Remind that a generic rotation matrix is a  $3 \times 3$  matrix defined as:

$$R = \begin{bmatrix} r_{11} & r_{12} & r_{13} \\ r_{21} & r_{22} & r_{23} \\ r_{31} & r_{32} & r_{33} \end{bmatrix} \quad (7)$$

where the trace is the sum of the elements on the main diagonal and it is invariant with respect to a change of basis:

$$tr(R) = r_{11} + r_{22} + r_{33} \quad (8)$$

After having computed the trace of the rotation matrix  $R_{13}^0$ , the angle  $\alpha$  is obtained from the following equation:

$$\alpha = \arccos\left(\frac{tr(R_{13}^0) - 1}{2}\right) \quad (9)$$

Now, the transformation matrix  $T_{13}^W$  can be evaluated:

$$T_{13}^W = \begin{bmatrix} \cos(\alpha) & -\sin(\alpha) & 0 & 0 \\ \sin \alpha & \cos(\alpha) & 0 & 0 \\ 0 & 0 & 1 & 0 \\ 0 & 0 & 0 & 1 \end{bmatrix} \quad (10)$$

Therefore, position and orientation of frame attached on each joint of the standing and swing leg (by applying an angular displacement of  $\pi$  on the actuated joint variable  $\theta'_1$ ) can be defined with the following transformation matrices<sup>1</sup>:

$$\begin{aligned} T_0^W &= T_{13}^W T_0^{13} \\ T_1^W &= T_0^W T_1^0 & T_1'^W &= T_0^W T_1'^0 \\ T_2^W &= T_1^W T_2^1 & T_2'^W &= T_1'^W T_2'^1 \\ T_3^W &= T_2^W T_3^2 & T_3'^W &= T_2'^W T_3'^2 \\ T_4^W &= T_2^W T_4^2 & T_4'^W &= T_2'^W T_4'^2 \\ T_5^W &= T_4^W T_5^4 & T_5'^W &= T_4'^W T_5'^4 \\ T_6^W &= T_5^W T_6^5 & T_6'^W &= T_5'^W T_6'^5 \end{aligned}$$

<sup>1</sup>Transformation matrices referred to swing leg are defined with apex

$$T_7^W = T_6^W T_7^6 \quad T_{7'}^W = T_{6'}^W T_{7'}^{6'}$$

$$T_8^W = T_5^W T_8^5 \quad T_{8'}^W = T_{5'}^W T_{8'}^{5'}$$

$$T_{13}^W = T_0^W T_{13}^0 \quad T_{13'}^W = T_7^W T_{13'}^{7'}$$

In this way, the gait pattern of swing foot and the body posture referred to the world frame have been obtained, as shown in Fig.4.2.7.

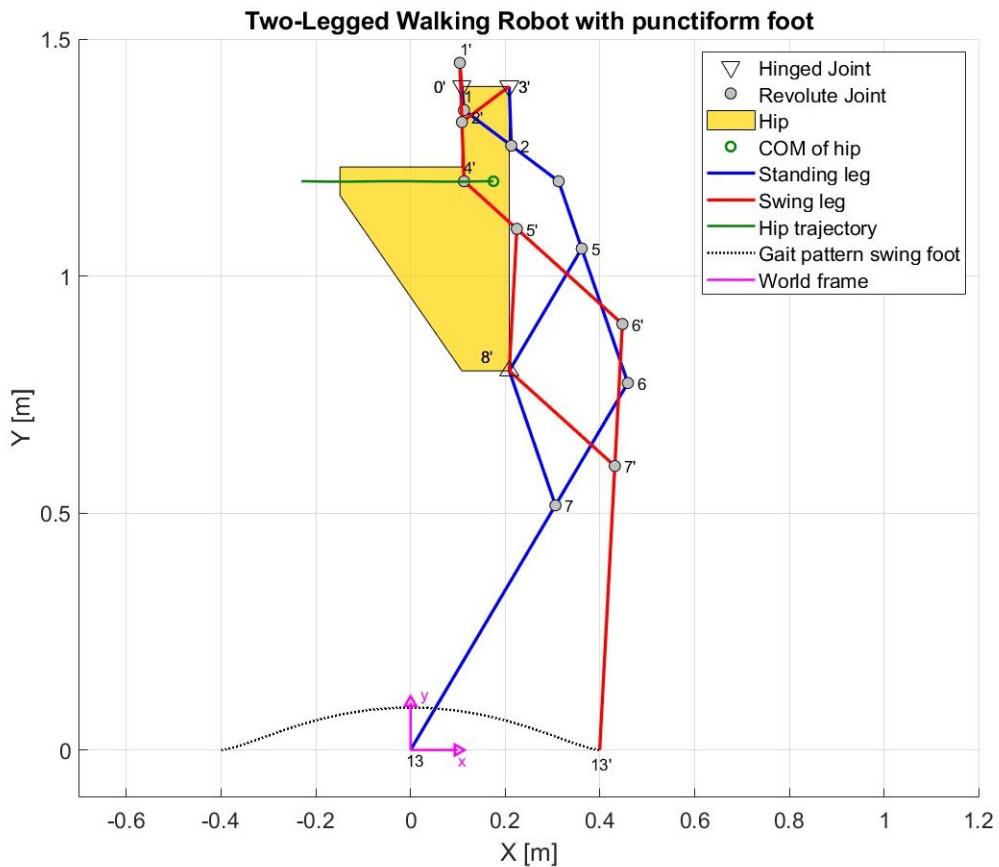


Figure 4.2.7: Body posture with punctiform foot

Moreover, a more realistic analysis of body posture need the presence of a foot with a fixed length. In order to do that, frame 0 of the standing leg has been referred to the new base frame  $FF$  attached on the toe by the transformation matrix:

$$T_0^{FF} = (T_{FF}^0)^{-1}$$

Then, the transformation matrix  $T_{FF}^W$  that express position and orientation of frame  $FF$  referred to frame  $W$ , is defined by computing  $\alpha$  from Eq.9 (subsituting the rotation matrix  $R_{13}^0$  with  $R_{FF}^0$ ,

rotation matrix extracted from  $T_{FF}^0$ ):

$$T_{FF}^W = \begin{bmatrix} \cos(\alpha) & -\sin(\alpha) & 0 & 0 \\ \sin \alpha & \cos(\alpha) & 0 & 0 \\ 0 & 0 & 1 & 0 \\ 0 & 0 & 0 & 1 \end{bmatrix} \quad (11)$$

After that, the transformation matrix  $T_0^W$  has been defined as:

$$T_0^W = T_{FF}^W T_0^{FF}$$

Transformation matrices that define position and orientation of frames attached to toe and heel respect to the world frame  $W$  are:

$$T_{FF}^W = T_{13}^W T_{FF}^{13} \quad T_{FF'}^W = T_{13'}^W T_{FF'}^{13'}$$

$$T_{BF}^W = T_{13}^W T_{BF}^{13} \quad T_{BF'}^W = T_{13'}^W T_{BF'}^{13'}$$

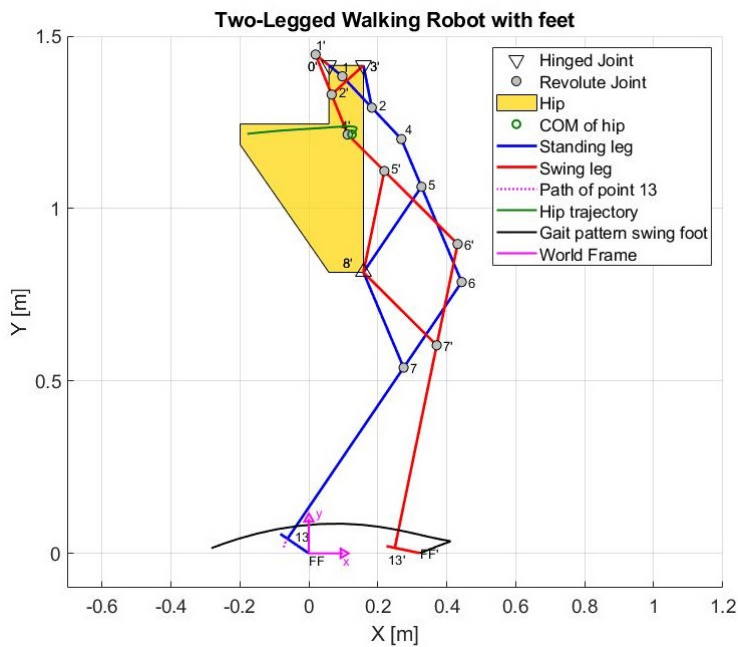


Figure 4.2.8: Body posture with foot of fixed length

In Fig.4.2.8 the body posture of two-legged walking robot equipped with feet is shown: the gait pattern of swing foot doesn't correspond to the ankle gait pattern (Fig.4.2.7 and this could cause instability during the walk: in fact, while the swing leg is going forward, the standing leg shouldn't rise up from the ground. Moreover, this cause a non-perfect traslational motion of the hip along the x-axis and, consequently, foot of the swing leg non parallel to the ground at the end of the swing phase. In order to avoid this problem and achieve the stability of biped during the walk, parallel extensions will be used.



### 4.3 Analysis with Parallel Extension

Same approach illustrated in 4.2 can be used to evaluate position and orientation of each link of the mechanism referred to the base frame 0, by using transformation matrices and following the Denavit-Hartenberg convention.

DH tables for the forward kinematics are proposed below.

| Frame | $a_i$ | $\alpha_i$ | $d_i$ | $\theta_i$    |
|-------|-------|------------|-------|---------------|
| 1     | L1    | 0          | 0     | $\theta_1$    |
| 4     | L2    | 0          | 0     | $\theta_2$    |
| 10    | L8    | 0          | 0     | $\theta_{10}$ |

Table 4.3.1: Denavit-Hartenberg table for first branch (0-1-4-10)

| Frame        | $a_i$ | $\alpha_i$ | $d_i$ | $\theta_i$ |
|--------------|-------|------------|-------|------------|
| $\tilde{1}0$ | L12   | 0          | 0     | $3\pi/2$   |
| $\hat{1}0$   | x     | 0          | 0     | $3\pi/2$   |

Table 4.3.2: Denavit-Hartenberg table for second branch (0-10-10)

| Frame | $a_i$ | $\alpha_i$ | $d_i$ | $\theta_i$    |
|-------|-------|------------|-------|---------------|
| 1     | L1    | 0          | 0     | $\theta_1$    |
| 4     | L2    | 0          | 0     | $\theta_2$    |
| 9     | L8/2  | 0          | 0     | $\theta_{10}$ |
| 11    | L9    | 0          | 0     | $\theta_9$    |

Table 4.3.3: Denavit-Hartenberg table for first branch (0-1-4-9-11)

| Frame        | $a_i$ | $\alpha_i$ | $d_i$ | $\theta_i$    |
|--------------|-------|------------|-------|---------------|
| 1            | L1    | 0          | 0     | $\theta_1$    |
| 4            | L2    | 0          | 0     | $\theta_2$    |
| 6            | L4    | 0          | 0     | $\theta_4$    |
| $\tilde{1}1$ | L10   | 0          | 0     | $\theta_{11}$ |

Table 4.3.4: Denavit-Hartenberg table for second branch (0-1-4-6-11)

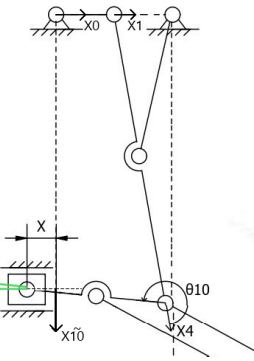


Figure 4.3.1: Frame's first loop

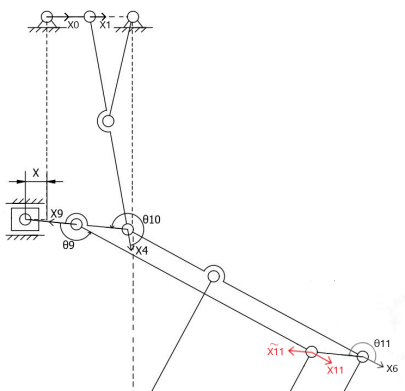


Figure 4.3.2: Frame's second loop



| Frame | $a_i$ | $\alpha_i$ | $d_i$ | $\theta_i$    |
|-------|-------|------------|-------|---------------|
| 1     | L1    | 0          | 0     | $\theta_1$    |
| 4     | L2    | 0          | 0     | $\theta_2$    |
| 6     | L4    | 0          | 0     | $\theta_4$    |
| 13    | L5    | 0          | 0     | $\theta_6$    |
| FF    | 1.5L  | 0          | 0     | $\theta_{13}$ |
| BF    | 4.1L  | 0          | 0     | $\pi$         |

Table 4.3.5: Denavit-Hartenberg table for first branch (0-1-4-6-13)

| Frame | $a_i$ | $\alpha_i$ | $d_i$ | $\theta_i$    |
|-------|-------|------------|-------|---------------|
| 1     | L1    | 0          | 0     | $\theta_1$    |
| 4     | L2    | 0          | 0     | $\theta_2$    |
| 9     | L8/2  | 0          | 0     | $\theta_{10}$ |
| 11    | L9    | 0          | 0     | $\theta_9$    |
| 12    | L11   | 0          | 0     | $\theta_{12}$ |
| 13    | L10   | 0          | 0     | $\theta_{13}$ |

Table 4.3.6: Denavit-Hartenberg table for second branch (0-1-4-9-11-12-13)

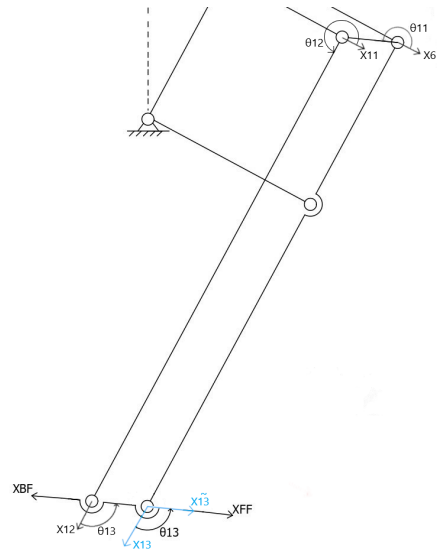


Figure 4.3.3: Frame's third loop

### 4.3.1 Closed Loop Equations

Three closed loop can be identified in the kinematic chain of the single leg with parallel extension, as shown in Fig.4.3.4.

Closure equation for first loop can be defined as follow:

$$p_{10}^0(q'_1) = p_{10}^0(q''_1) \quad (12)$$

where

$$q'_1 = [\theta_1 \quad \theta_2 \quad \theta_{10}] \quad q''_1 = [3\pi/2 \quad 3\pi/2 \quad x]$$

Closure equation for second loop can be defined as follow:

$$p_{11}^0(q'_2) = p_{11}^0(q''_2) \quad (13)$$

where

$$q'_2 = [\theta_1 \quad \theta_2 \quad \theta_{10} \quad \theta_9] \quad q''_2 = [\theta_1 \quad \theta_2 \quad \theta_4 \quad \theta_{11}]$$

Closure equation for third loop can be defined as follow:

$$p_{13}^0(q'_3) = p_{13}^0(q''_3) \quad (14)$$

where

$$q'_3 = [\theta_1 \quad \theta_2 \quad \theta_4 \quad \theta_6] \quad q''_3 = [\theta_1 \quad \theta_2 \quad \theta_{10} \quad \theta_9 \quad \theta_{12} \quad \theta_{13}]$$

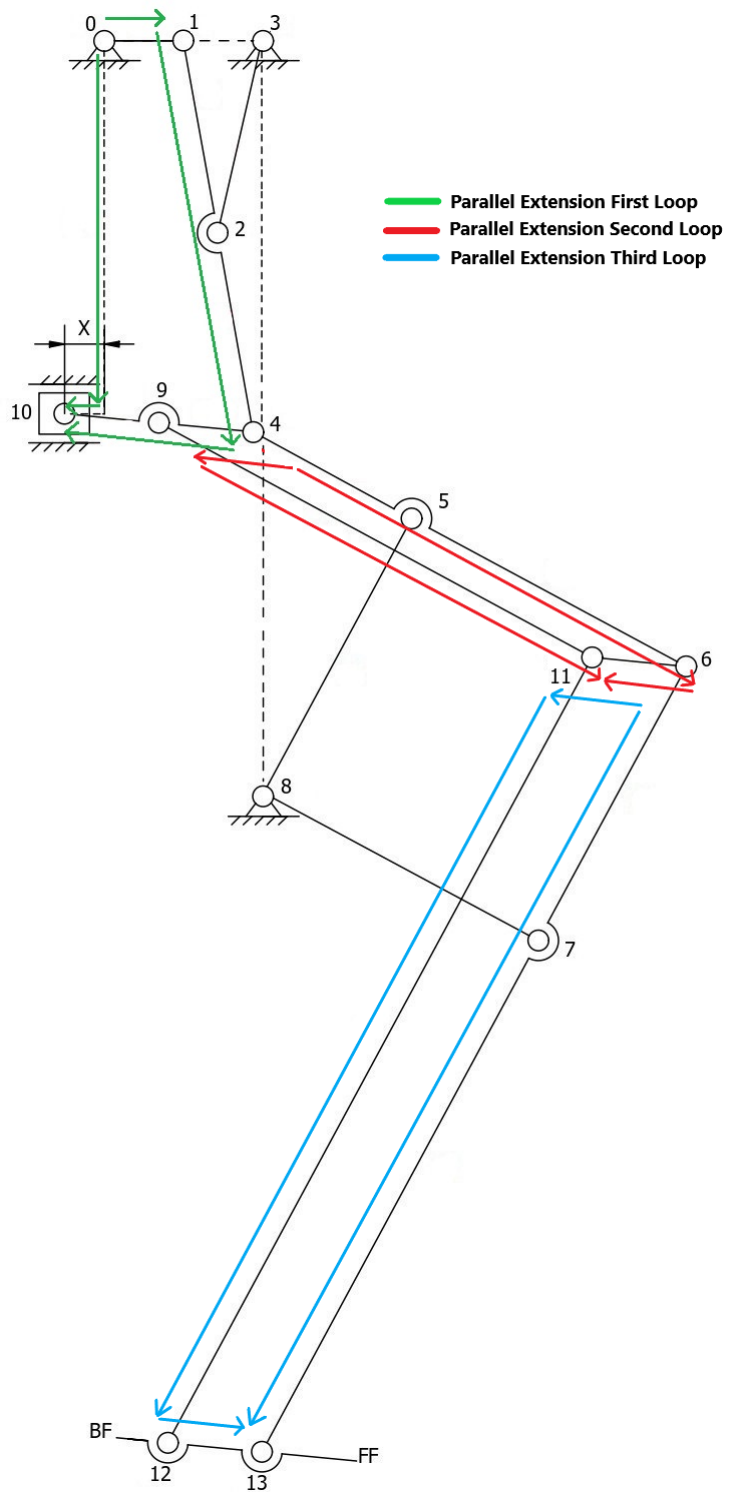


Figure 4.3.4: Closed loop leg mechanism with parallel extension

### 4.3.2 Simulation and Results

By solving Eq.12, Eq.13 and Eq.14, all joint variables of the mechanism are determined, so it's possible to compute the pose of foot respect to the base frame 0.

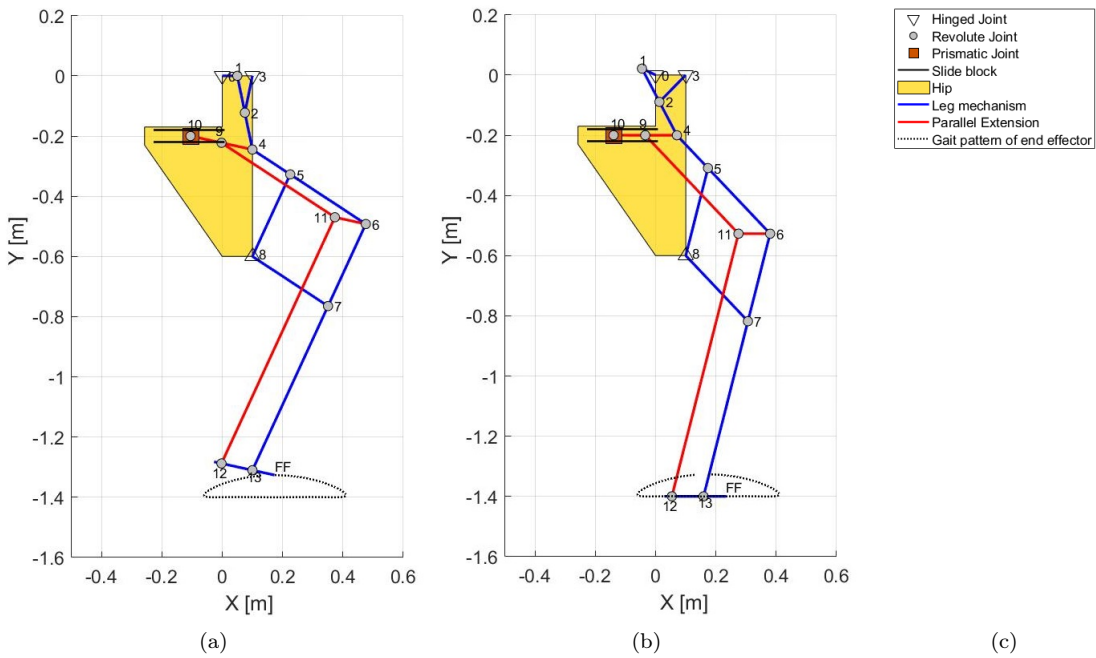


Figure 4.3.5: Gait pattern of toe using parallel extension

Fig 4.3.5 shows the gait pattern of toe when the leg is equipped with a parallel extension. The main result of this simulation is that the parallel extension keeps the foot parallel to the ground during the straight-line portion, in opposition to what happens in Fig.4.2.6.

### 4.3.3 Body Posture Analysis In Walking Phase

Body posture with a parallel extension can be analyzed using same concepts described in 4.2. Once determined the transformation matrix

$$T_0^{FF} = (T_{FF}^0)^{-1}$$

the rotation angle  $\alpha$  can be computed from the rotation matrix extracted from  $T_{FF}^0$ . After that, the transformation matrix  $T_{FF}^W$  can be defined as shown in Eq.11 and  $T_0^W$  consequently.

### 4.3.4 Simulations and Results

In Fig.4.3.6 three snapshot of a step are shown, in particular the first one refers to the toe-off phase (Fig. 4.3.6a) in which the foot of the swing leg prepares to leave, rising heel first and toe next; the second one is the leg-lift phase (Fig. 4.3.6b) in which the foot has completely left the ground; the last one is the swing phase (Fig. 4.3.6c) in which the standing leg allow the swing leg to move forward.

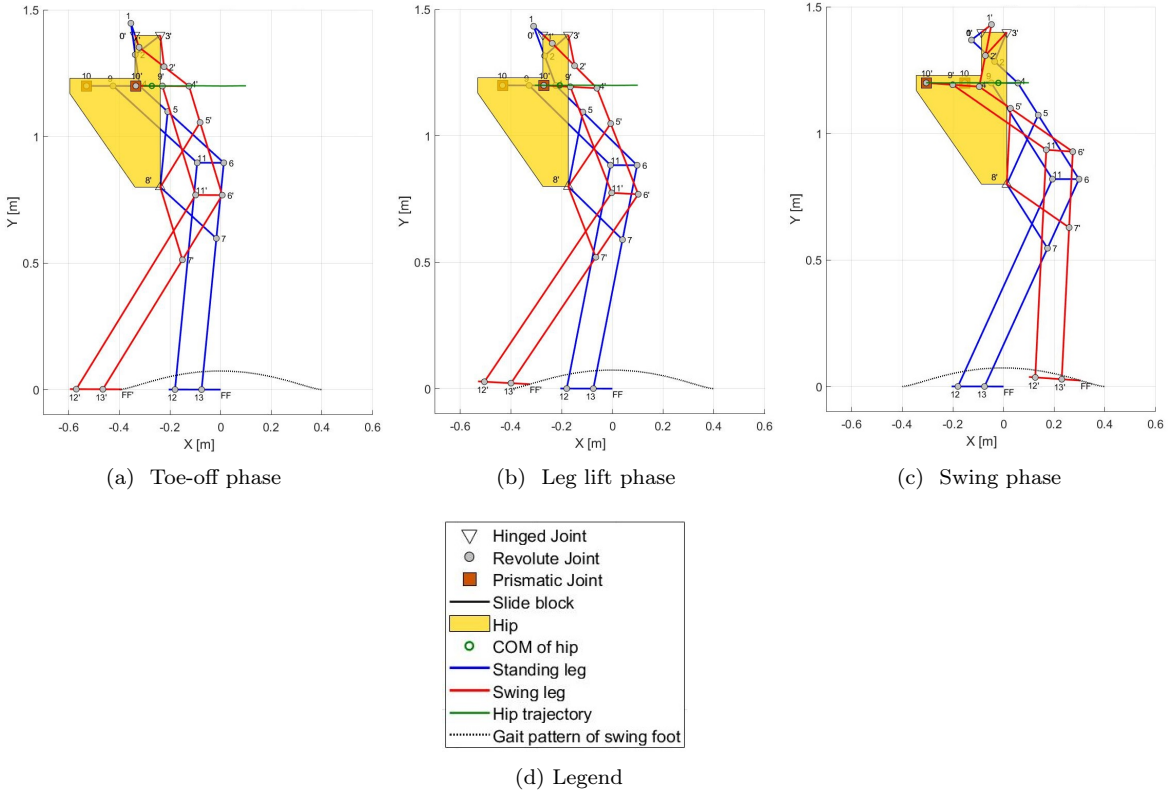


Figure 4.3.6: Body posture with parallel extension

As can be seen in Fig.4.3.6 , the use of parallel extensions for each leg mechanism allows the foot of swing leg to be parallel to the ground both at the beginning of the toe-off phase and at the end of the swing phase and also allows to keep the foot of standing leg in contact with the ground and parallel to it in each phase.

Moreover, it improves the hip trajectory (that is purely traslational along x-axis of the world frame) on the sagittal plane respect to the leg configuration without parallel extensions (Fig.4.2.8).



## 5 Differential Kinematics

Differential kinematics gives the relationship between the joint velocities and the corresponding end-effector linear and angular velocity [8]. This relationship is given by a matrix, named geometric Jacobian, which depends on the mechanism configuration. Defined  $\dot{\mathbf{p}}_e$  the end effector linear velocity and  $\mathbf{w}_e$  the angular velocity, equations that lead these to the joint velocities  $\dot{\mathbf{q}}_i$  are:

$$\dot{\mathbf{p}}_e = \mathbf{J}_P(\mathbf{q})\dot{\mathbf{q}} \quad (15)$$

$$\mathbf{w}_e = \mathbf{J}_O(\mathbf{q})\dot{\mathbf{q}} \quad (16)$$

where  $\mathbf{J}_P$  is a  $3 \times n$  matrix that relates the joint velocities with the end effector linear velocities, whereas  $\mathbf{J}_O$  is also  $3 \times n$  matrix that links the joint velocities to the end effector angular velocity. The geometric Jacobian matrix is obtained matching the previous two matrices, resulting in a  $6 \times n$  matrix (where  $n$  is the number of joint variables) defined as:

$$\mathbf{J} = \begin{bmatrix} \mathbf{J}_{P1} & \mathbf{J}_{P2} & \dots & \mathbf{J}_{Pn} \\ \mathbf{J}_{O1} & \mathbf{J}_{O2} & \dots & \mathbf{J}_{On} \end{bmatrix} \quad (17)$$

If the  $i - th$  joint is prismatic the geometric Jacobian matrix can be computed as:

$$\begin{bmatrix} \mathbf{J}_{Pi} \\ \mathbf{J}_{Qi} \end{bmatrix} = \begin{bmatrix} \mathbf{z}_{i-1} \\ \mathbf{0} \end{bmatrix} \quad (18)$$

while if it is a revolute joint:

$$\begin{bmatrix} \mathbf{J}_{Pi} \\ \mathbf{J}_{Qi} \end{bmatrix} = \begin{bmatrix} \mathbf{z}_{i-1} \times (\mathbf{p}_e - \mathbf{p}_{i-1}) \\ \mathbf{z}_{i-1} \end{bmatrix} \quad (19)$$

In Eq.18 and Eq.19 all terms are given by transformation matrices, in particular:

- $\mathbf{z}_{i-1}$  is the z-axis, corresponding to the third column of rotation matrix  $R_{i-1}^0$ ;
- $\mathbf{p}_e$  is the position vector of the end effector respect to the base frame 0, corresponding to the first three element of the fourth column of transformation matrix  $T_e^0$ ;
- $\mathbf{p}_{i-1}$  is the position vector of the origin of frame  $i - 1$  respect to the base frame 0, corresponding to the first three element of the fourth column of transformation matrix  $T_{i-1}^0$ .

Whenever the mechanism contains a closed chain, its structure is transformed into a tree-structured open chain by virtually cutting the loop at a joint (it's preferred to consider unactuated joints). Then, it must be considered the number of joint variables of the open chain obtained.

In the study case, the leg mechanism is virtually cut at the joint 2, 5 and 7. The open chain obtained has four joint variables:  $\theta_1, \theta_2, \theta_4, \theta_5$ . As a consequence, the geometric Jacobian that must be computed is a  $6 \times 4$  matrix.

After having computed the geometric Jacobian for the leg mechanism with a base frame placed in joint 0, linear velocity and acceleration of the end effector (joint 13) has been obtained considering a motor crank with angular velocity of  $0.1 \text{ rad/s}$ .

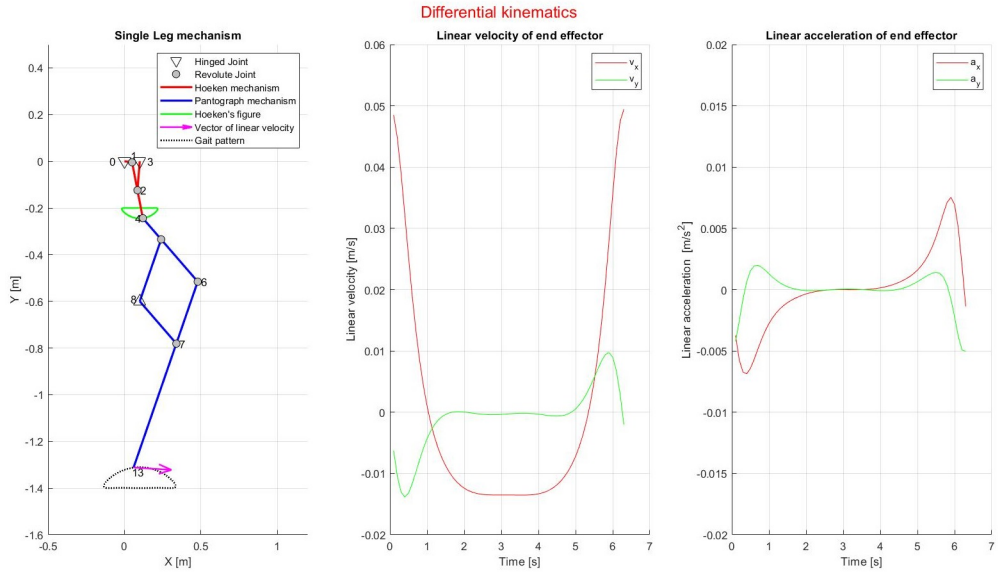


Figure 5.1: Linear velocity and acceleration of end effector (ankle joint)

As expected, simulation in Fig.5.1 shows that during the straight-line portion of gait pattern, the end effector linear velocity is almost constant: in particular, the x component  $v_x$  is constant and assumes negative values whereas the y component  $v_y$  is around 0. As a consequence, linear acceleration of end effector in the straight-line portion is nearly constant and equal to 0 while in the elliptic path has a non-zero value.



## 6 Autodesk Inventor Professional 2020

Autodesk Inventor is a computer-aided design application for 3D mechanical design, simulation, visualization, and documentation developed by Autodesk. Inventor allows 2D and 3D data integration in a single environment, creating a virtual representation of the final product that enables users to validate the form, fit, and function of the product before it is ever built.

### 6.1 Prototype of Walking Robot

After having defined length of each link of the walking robot and a possible hip shape, the prototype of walking robot has been defined, as shown in Fig. 6.1.1.

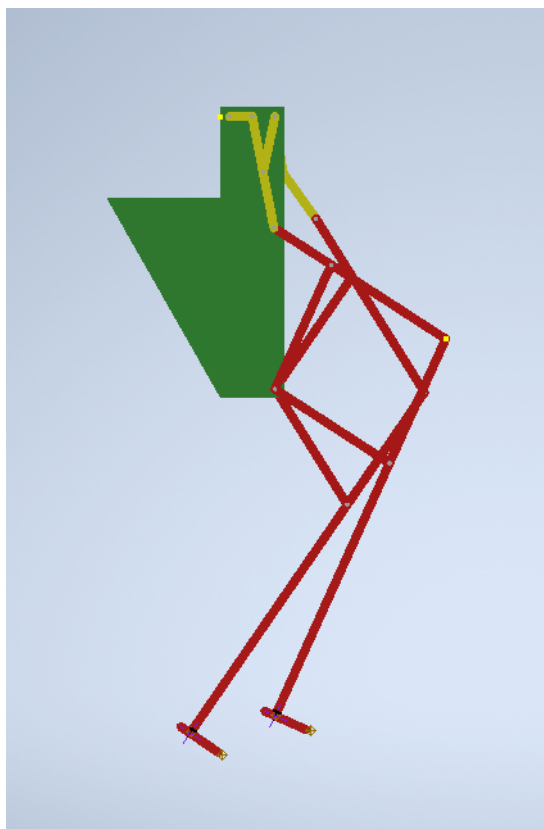


Figure 6.1.1: Prototype of walking robot in Inventor Pro 2020

One of the feature of Inventor Pro 2020 is the possibility to animate a specific joint's variable in order to compute path of a specific point of the mechanism and also linear velocity and acceleration profile of that point. Thus, it's necessary to define the CAD model of the mechanism, choosing the right kinematic pairs.

### 6.2 Path of Ankle and Toe

By defining the angular velocity of motor crank of the leg mechanism equal to  $1 \text{ rad/s}$ , gait pattern of ankle and toe respect to base frame attached to joint 0 has been computed, as shown in Fig. 6.2.1.

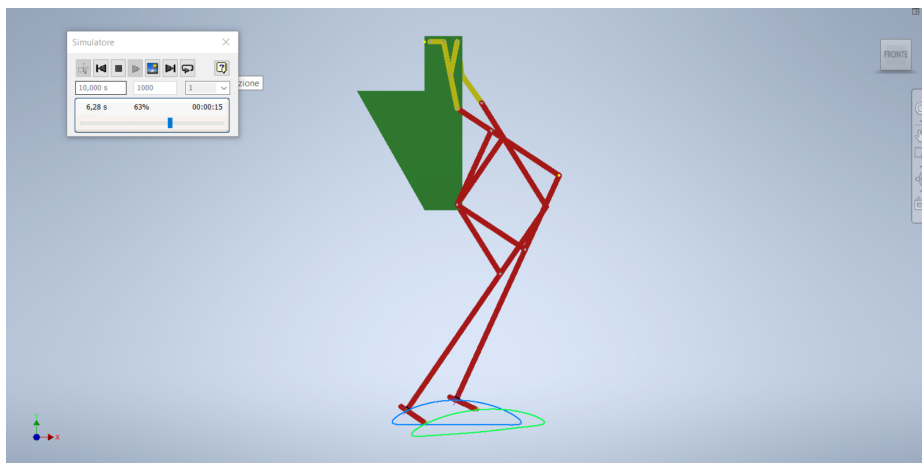


Figure 6.2.1: Path of ankle and toe

As can be seen, the gait pattern of the ankle is quite different respect to the toe one: in particular, the gait pattern of toe has the straight-line portion that isn't parallel to the ground which could determine instability of the walking robot during the walking phases, as discussed in the previous sections.

### 6.3 Linear Velocity and Acceleration of the Ankle

By changing the angular velocity to  $0.1 \text{ rad/s}$ , linear velocity and acceleration of the ankle respect to the base frame 0 are computed.

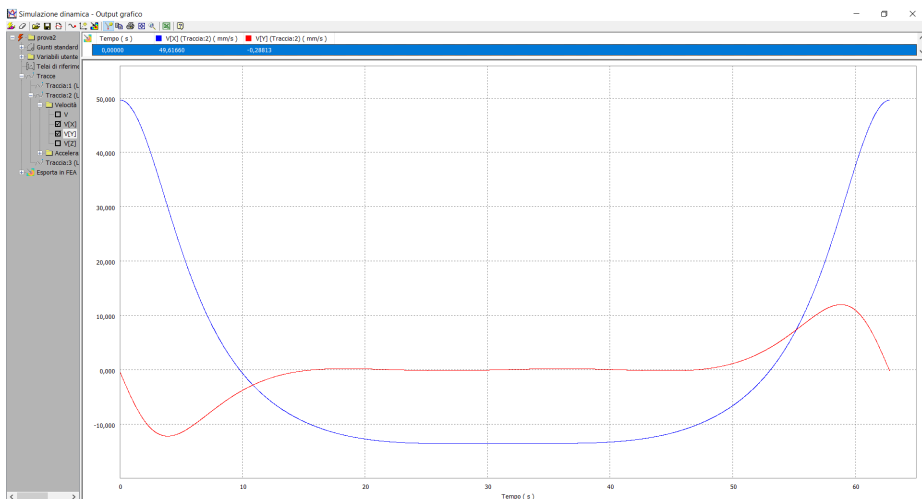


Figure 6.3.1: Linear velocity of ankle

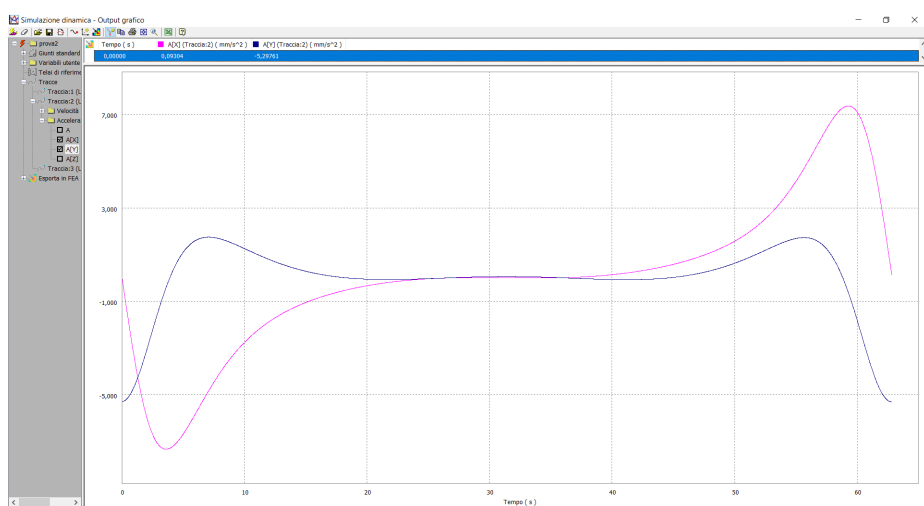


Figure 6.3.2: Linear acceleration of ankle

As can be seen in Fig.6.3.1 and Fig.6.3.2, results obtained in Autodesk Inventor are the same given by Matlab simulations in terms of path, velocity and acceleration profiles.

## 7 Inverse Dynamics

Inverse dynamics is a method for computing forces and/or moments of force (torques) based on the kinematics (motion) of a body and the body's inertial properties (mass and moment of inertia). As discussed in Section 4.3.3, a parallel extension can improve stability on the sagittal plane of the walking robot. This solution is affected by an increasing of the number of links and revolute joints. Thus, in the following sections another solution is proposed, where torsion spring is placed in each ankle's joint in order to improve robot stability, avoiding the use of an additional actuator or a stabilizer mechanism.

As a consequence, the aim of this analysis is to determine torques  $T_a$  and  $T_e$  provided by the actuator and the spring, respectively, and the spring torsion coefficient  $K_e$ , in order to follow the kinematic behavior discussed in the previous sections.

Few hypotheses have been considered, allowing the simplification of the problem:

- mass of each link is concentrated in its geometrical center;
- supporting foot is not allowed to slip;
- friction in kinematic pairs is not considered.

### 7.1 Mass Distribution

In order to formulate a dynamic model, it's important to define mass distribution of each link of the mechanism: in particular, a concentrated mass in the geometrical center of each link has been considered, as can be seen in Fig.7.1.1.

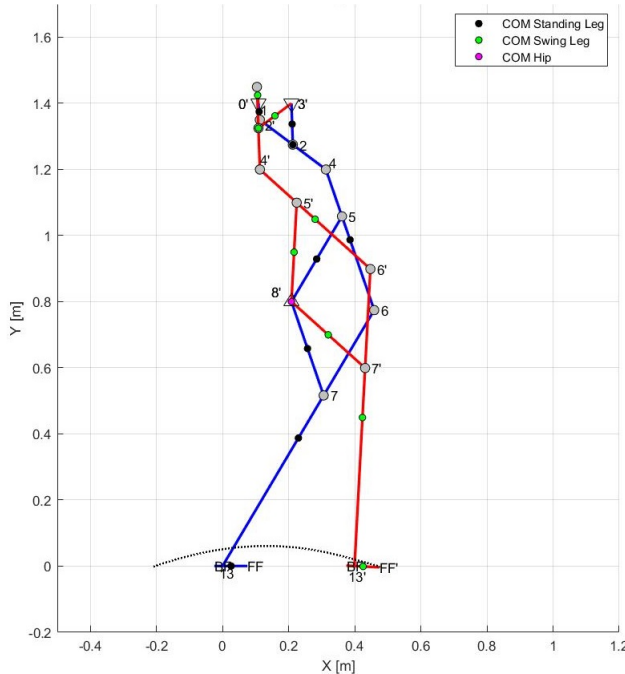


Figure 7.1.1: Mass distribution and center of mass of links

A first approximation of mass distribution of walking robot can be done considering the human body one, referring to the table in [9] in which the mass of each part of human body is defined as percentage of total mass.



|       | % of total mass |
|-------|-----------------|
| Hip   | 25              |
| Thigh | 10              |
| Shank | 5               |
| Foot  | 2               |

Table 7.1.1: Mass distribution of human body

The total mass of the walking robot is defined equal to 65 kg.

Considering that groups of links imitate part of human body, several analogies can be found:

- links L1, L2, L3, L4 and L6 act as thigh
- links L5 and L7 act as shank
- links that define toe and heel of feet act as foot

In order to compute the mass of each link a weighted average has been considered. For instance, considering the thigh that is defined by links L1, L2, L3, L4 and L6, mass of those links are defined using the following equation:

$$m_i = \frac{l_i M_{thigh}}{l_1 + l_2 + l_3 + l_4 + l_6} \quad i = 1, 2, 3, 4, 6$$

Same method is used to compute masses of the other links. At the end, mass distribution of walking robot is determined and reported in Tab.7.1.2:

|      | Mass [Kg] |
|------|-----------|
| Hip  | 16        |
| L1   | 0.3       |
| L2   | 1.4       |
| L3   | 0.7       |
| L4   | 2.5       |
| L5   | 2.4       |
| L6   | 1.7       |
| L7   | 0.8       |
| Foot | 1.3       |

Table 7.1.2: Mass distribution of walking robot



## 7.2 Torsion Spring

A torsion spring is a spring that works by twisting its end along its axis; that is, a flexible elastic object that stores mechanical energy when it is twisted. When it happened, it exerts a torque in the opposite direction, proportional to the amount (angle) it is twisted. As long as they are not twisted beyond their elastic limit, torsion springs obey an angular form of Hooke's law:

$$T_e = -K_e \Delta\beta$$

where  $T_e$  [Nm] is the torque exerted by the spring and  $\Delta\beta$  [rad] is the angle of twist from its equilibrium position.  $K_e$  [Nm/rad], variously called the spring's torsion coefficient, torsion elastic modulus, rate, or just spring constant, is equal to the change in torque required to twist the spring through an angle of 1 radian and it is analogous to the spring constant of a linear spring. The negative sign indicates that the direction of the torque is opposite to the direction of twist.



Figure 7.2.1: Torsion Spring

Notice that a torsion spring has its own winding direction, which is unique. If it is stressed in the opposite direction over the yield point, the spring might not be able to return to its initial configuration because of plastic deformation.

## 7.3 Quasi-Static

To determine torsion spring coefficient, a quasi-static model has been considered, using the Newton-Euler formulation, in which the mechanism is moving so slowly that it can be considered static. Thus, force and moment of inertia are excluded in this analysis.

### 7.3.1 Equation of Motion

Newton-Euler equations is the grouping together of Euler's two laws of motion for a rigid body with a plane motion:

$$\begin{cases} \sum_i \mathbf{F}_i = m\mathbf{a}(P_0) \\ \sum_i [(\mathbf{P}_i - \mathbf{O}) \times \mathbf{F}_i + \mathbf{T}_i] = I(O)\dot{\boldsymbol{\omega}} \end{cases} \quad (20)$$

where  $P_0$  is the center of mass of rigid body and  $O$  is a reduction pole of moments.



Following the hypotheses above, a free body diagram can be done, writing Newton-Euler equations for the  $n$  rigid bodies of the walking robot:

$$\begin{cases} \sum_j [\mathbf{F}_{ji} + m_i \mathbf{g}] = 0 \\ \sum_j [\mathbf{r}_{ik} \times \mathbf{F}_{ji} + \mathbf{T}_i] = 0 \end{cases} \quad (21)$$

for  $i = 1, \dots, n$ , where

- $\mathbf{F}_{ji}$  is the force exerted by the  $j - th$  link on the  $i - th$  link;
- $\mathbf{T}_i$  is the torque applied on the  $i - th$  link;
- $\mathbf{r}_{ik}$  is the position vector from the center of mass  $i$  to the point of application  $k$  of  $\mathbf{F}_{ij}$ ;
- $m_i$  is the mass of link  $i$ .

In Fig.7.3.1 an example of a free body diagram for the  $i - th$  link is shown.

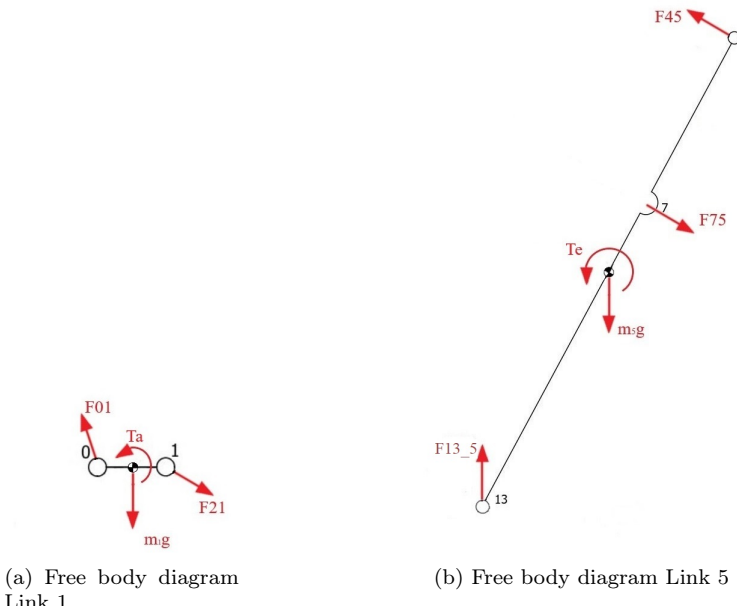


Figure 7.3.1: Examples of free body diagram

Therefore, a system of  $3n$  linear equations can be written, where the unknowns are represented by forces and torques exchanged between each link. In particular, the first two equations are led to the first cardinal equation of dynamics while the third one is led to the second cardinal equation. A compact expression of Eq.21 in a matrix form could be written as follow:

$$\begin{bmatrix} a_{11} & a_{12} & \dots \\ a_{21} & a_{22} & \dots \\ \dots & \dots & a_{48,48} \end{bmatrix} \begin{bmatrix} F_{12x} \\ F_{12y} \\ \dots \\ T_a \\ T_e \end{bmatrix} + \begin{bmatrix} \dots \\ m_1 g \\ \dots \\ \dots \end{bmatrix} = 0 \quad (22)$$

that is:

$$AF = b \quad (23)$$

where  $A$  is a  $48 \times 48$  coefficient matrix which dimension depends on the number of rigid bodies of the robot,  $F$  is the unknown vector of forces and torques,  $b$  is the known vector. By inverting the coefficient matrix  $A$ , the unknown vector  $F$  in Eq.23 can be easily computed:

$$F = A^{-1}b$$

Notice that the free body diagram of the supporting foot has not been considered because the determination of the point of application of the force exchanged between foot and ground requires a deeper analysis, in particular it must be known the plantar pressure distribution when foot of the standing leg get in contact with the ground.

### 7.3.2 Simulation and Results

Relevant simulation outputs such as actuated and elastic torques of each leg have been plotted respect to the ankle joint's angle  $\beta$ , as shown in Fig.7.3.2. Masses and links' length used in this simulation can be found in Tab.7.1.2 and Tab.3.6.1, respectively.

In the following simulation, a center of mass of the hip placed in the same position of joint 8 has been considered (Fig.7.3.2). Changing the position of center of mass, the elastic torque necessary to the static equilibrium of the mechanism will change.

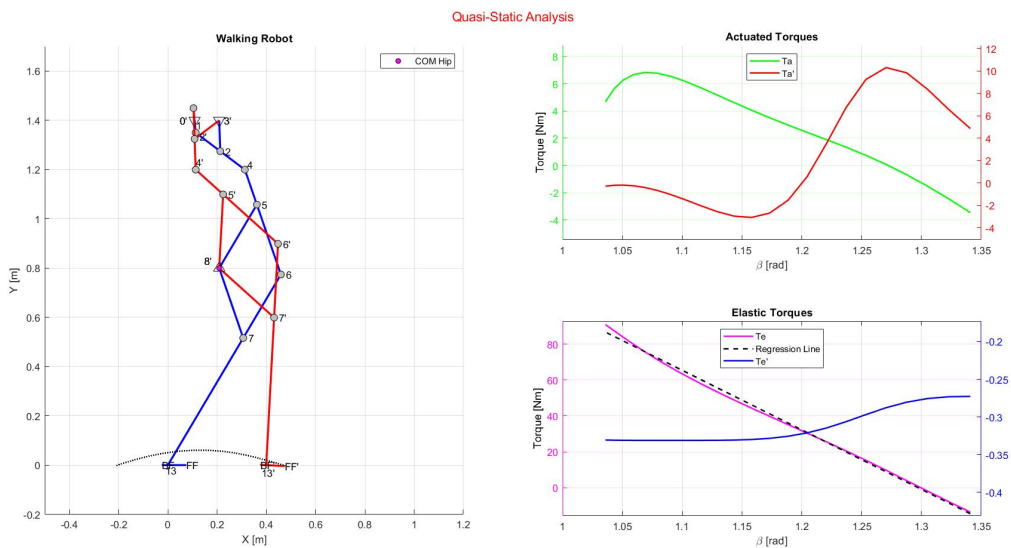


Figure 7.3.2: Torques

In Fig.7.3.2, the elastic torque  $T_e$  of the standing leg is nearly linear, while the swing leg one is negligible. Thus, in order to compute a spring coefficient  $K_e$  approximation , a linearization of  $T_e$  has been considered using the least squares method. Therefore, according to the relation:

$$T_e = -K_e \Delta\beta$$

where  $\Delta\beta = \beta - \beta_0$ <sup>1</sup> is the angle of twist of the spring from its equilibrium position (Fig.7.3.3),  $K_e$  can be derived by the slope of the regression line in Fig.7.3.2.

<sup>1</sup> $\beta_0$  is the angle between foot and tibia at the beginning of toe-off phase (around 80 degree).

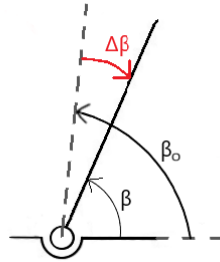


Figure 7.3.3: Twist angle  $\Delta\beta$

The output of this simulation is a torsion spring coefficient equal to around  $330 \text{ Nm/rad}$ .

## 7.4 Dynamic Analysis

A more accurate model is mandatory in order to obtain feasible value of actuated torques, so forces and moments of inertia must be considered.

### 7.4.1 Equation of motion

System of equations in Eq.21 can be written in a complete form such as:

$$\begin{cases} \sum_j [\mathbf{F}_{ji} + m_i \mathbf{g}] = m \mathbf{a}_i \\ \sum_j [\mathbf{r}_{ik} \times \mathbf{F}_{ji} + \mathbf{T}_i] = I_i \dot{\omega}_i \end{cases} \quad (24)$$

for  $i = 1, \dots, n$ , where

- $\mathbf{F}_{ji}$  is the force exerted by the  $j - th$  link on the  $i - th$  link;
- $\mathbf{T}_i$  is the torque applied on the  $i - th$  link;
- $\mathbf{a}_i$  is the linear acceleration of center of mass of  $i - th$  link;
- $\dot{\omega}_i$  is the angular acceleration of  $i - th$  link;
- $I_i$  is the moment of inertia referred to the center of mass of the  $i - th$  link ;
- $\mathbf{r}_{ik}$  is the position vector from the center of mass  $i$  to the point  $k$  of application of  $\mathbf{F}_{ij}$ ;
- $m_i$  the mass of  $i - th$  link .

Due to hypotheses mentioned at the beginning of this chapter, mass of each link is concentrated in its geometrical center, so moment of inertia  $I_i$  referred to it is null. Therefore, same consideration can be done as in Section 7.3 in order to compute actuated and elastic torques, and the spring coefficient.

Different simulations have been taken into account, by varying angular velocity  $\omega_1$  of the motor crank, center of mass and mass of the hip (having almost the entire mass of the robot).

#### 7.4.2 Simulation and Results - First Simulation

In the first simulation the angular velocity of the motor crank  $\omega_1$  has been set to  $0.1 \text{ rad/s}$  and the mass of the hip has been set to  $16 \text{ kg}$  with COM coincident to joint 8, as can be seen in Fig.7.4.1.

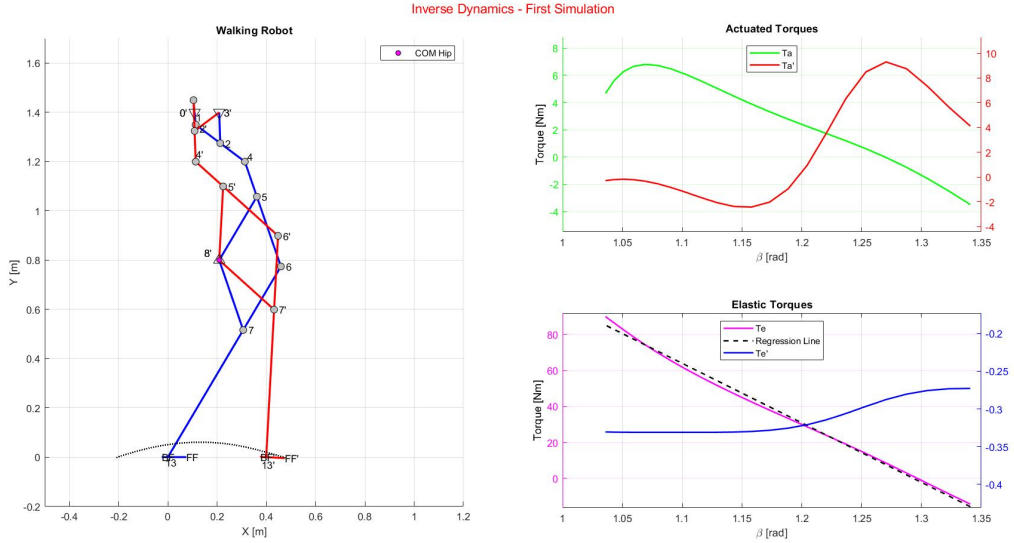


Figure 7.4.1: First Simulation

The spring coefficient, derived by the slope of the regression line, is:

$$K_e \simeq 331 \text{ Nm/rad}$$

At the beginning of the simulation (when the foot of swing leg has just left the ground), the elastic torque of the standing leg has negative values because the COM of the hip is on the left side respect to the support foot. When the COM of the hip falls in the area of the foot in contact with the ground, the elastic torque of the standing leg changes sign, having positive values.

#### 7.4.3 Simulation and Results - Second Simulation

In the second simulation the angular velocity of the motor crank  $\omega_1$  has been set to  $0.1 \text{ rad/s}$  and the mass of the hip has been set to  $16 \text{ kg}$  with COM shifted forward respect to the first simulation, as can be seen in Fig.7.4.2.

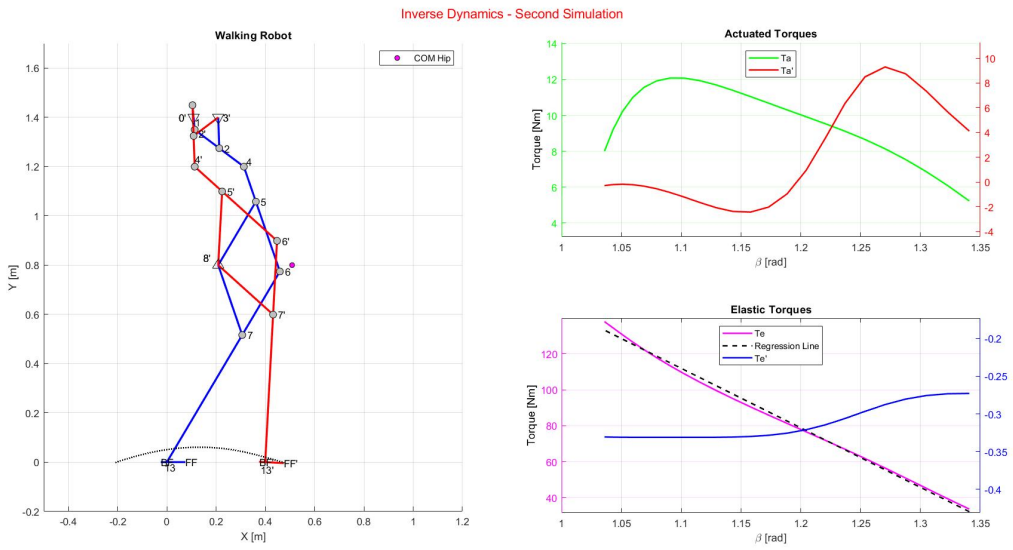


Figure 7.4.2: Second Simulation

In this case, still at the beginning of the simulation, the elastic torque of the standing leg has positive values due to the position of COM of the hip.

Moreover, it can be seen that the behaviour of torsion spring is almost linear. In particular, the spring coefficient is:

$$K_e \simeq 331 \text{ Nm/rad}$$

#### 7.4.4 Simulation and Results - Third Simulation

In the third simulation the angular velocity of the motor crank  $\omega_1$  has been set to  $0.1 \text{ rad/s}$  and the mass of the body has been set to  $30 \text{ kg}$  with COM shifted in the same direction of walking with respect to the first simulation, as can be seen in Fig.7.4.3.

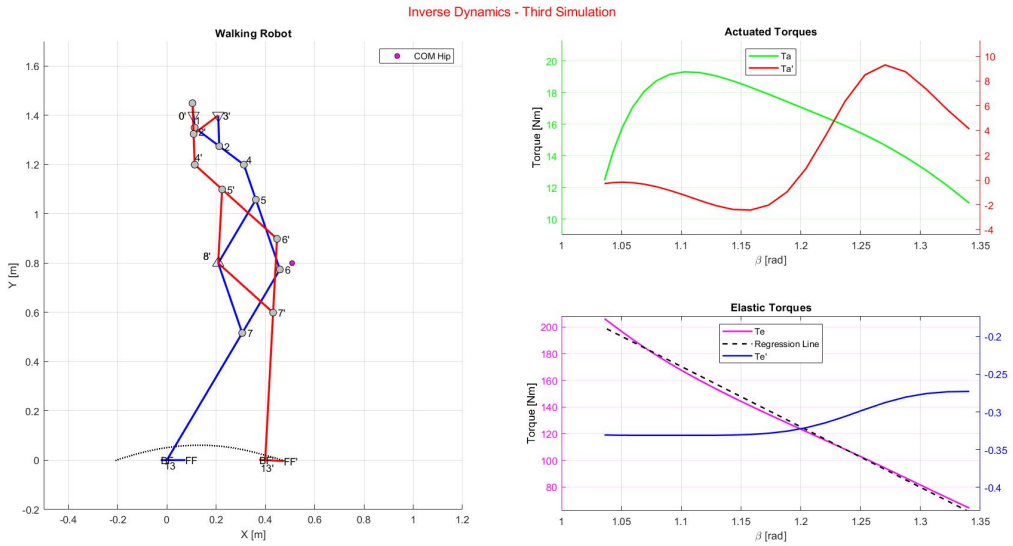


Figure 7.4.3: Third Simulation

Fig.7.4.3 shows that increasing the mass of the body up to  $30 \text{ kg}$  has increased the slope of regression line, so the spring coefficient has a higher value than in the previous simulations. More in depth, spring coefficient is:

$$K_e \simeq 453 \text{ Nm/rad}$$

Another interesting result is that the actuated torque of the standing leg has increased, as expected.

#### 7.4.5 Simulation and Results - Fourth Simulation

In the last simulation, the angular velocity of the motor crank  $\omega_1$  has been increased up to  $5 \text{ rad/s}$  and the mass of the hip has been set to  $20 \text{ kg}$  with COM shifted in the same direction of walking with respect to the first simulation, as can be seen in Fig.7.4.4.

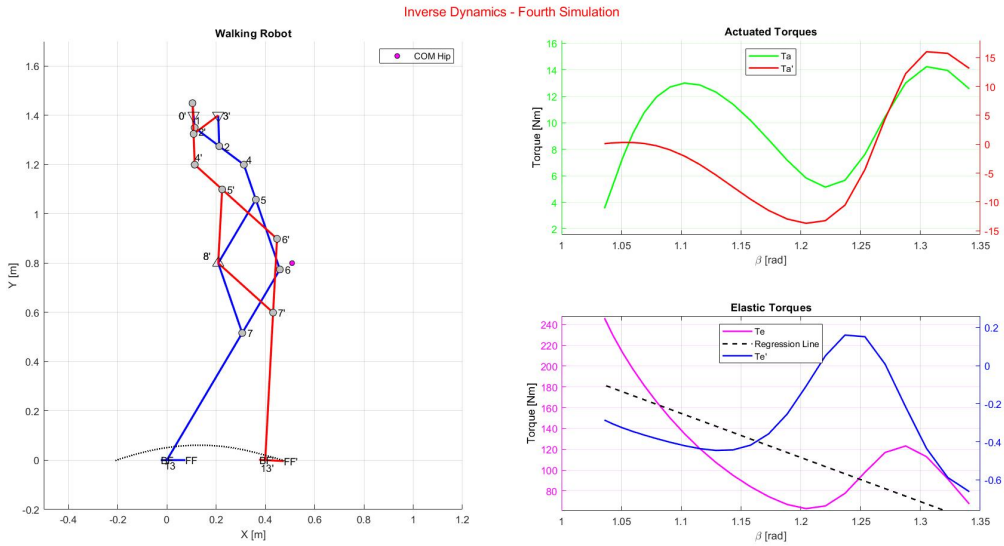


Figure 7.4.4: Fourth Simulation

Main result of this simulation is represented by a non-linear elastic torque of the standing leg due to the increasing of the accelerations  $a_i$ , corresponding to a more relevant contribution of forces of inertia. For this reason, spring coefficient computed in this simulation may be incorrect. For the sake of completeness, spring coefficient is:

$$K_e \simeq 424 \text{ Nm/rad}$$



## 8 Conclusions & Future Works

In this project it has been chosen to direct our efforts on reducing the number of degrees of freedom, and consequently the number of actuators, in order to improve power consumption and at the same time keeping a feasible walking gait. In order to do this, the walking robot has been defined as combination of classical mechanisms: in particular Hoeken linkage has been used as quasi straight-line generator mechanism and pantograph as amplifier mechanism). The original model presented also a parallel extension for each leg that allows to keep the foot of standing leg in contact with the ground and parallel to it. Due to the higher number of links and revolute joints of this model, the parallel extension has been replaced with a torsion spring between tibia and foot. Dynamics analysis of this kind of walking robot has been done, computing the required elastic torque of the standing leg in order to avoid instability of the biped. Moreover, using a CAD environment like Inventor Pro 2020, simulations derived by MATLAB scripts, have been verified.

Future works could be focused on different improvements.

- sizing each rigid body of the robot in a more precise way, considering, for example, a realistic masses distribution;
- designing a transmission system that can reduce the number of actuators from 2 to 1, by providing a displacement of  $\pi \text{ rad}$  between the angular position of the two cranks;
- studying the behavior of the robot also on the frontal plane;



## References

- [1] "MUSME 2011, 4 th International Symposium on Multibody Systems and Mechatronics". In: *Editorial Universitat Politècnica de València* (2011).
- [2] Oliver Jones. *Walking and gaits*. May 2019. URL: <https://teachmeanatomy.info/lower-limb/misc/walking-and-gaits/>.
- [3] Valeriy Tereshin Anastasiya Borina. "HISTORY OF BIPED ROBOTS.PROBLEMS.SOLUTIONS". In: *History of Mechanism and Machine Science* (2015).
- [4] Giuseppe Carbone LARM: Laboratory of Robotics Conghui Liang Marco Ceccarelli and University of Cassino Mechatronics. "Design and Simulation of Legged Walking Robots in MATLAB® Environment". In: *History of Mechanism and Machine Science* (2014).
- [5] J.C. García-Prada E. Corral J. Meneses. "Forward and Inverse Dynamics and Quasi-Static Analysis of Mechanizes with MATLAB®". In: *MAQLAB group, Universidad Carlos III de Madrid, Spain* (2016).
- [6] Robert L. Norton. *Design of Machinery - An Introduction to the Synthesis and Analysis of Mechanisms and Machines*. McGraw-Hill Series in Mechanical Engineering. McGraw-Hill, 1998.
- [7] J.C. Garcia-Prada M.E Escobar H.Rubio. "Analysis of the Stabilization System of Mimbot Biped". In: *Editorial Universitat Politècnica de València* (2012), Journal of applied research and tecnology.
- [8] L.Villani B.Siciliano L.Sciavicco. *Robotics, Modelling, Planning and Control*. Third edition. Mc-GrawHill, 2008. ISBN: 978-88-386-6322-2.
- [9] George R.L Gaughran Wilfrid Taylor Dempster. "Properties of body segments based on size and weight". In: *Department of Anatomy, university of Michigan* (1967).



## List of Figures

|       |  |    |
|-------|--|----|
| 2.1   | Walking phases . . . . .   | 5  |
| 2.2   | Mechanical knight of Leonardo da Vinci . . . . .                         | 6  |
| 2.3   | Chebyshev multiple-bar walking mechanism . . . . .                       | 7  |
| 2.4   | WAP-1 walking robot . . . . .  | 7  |
| 2.5   | WAP-3 walking robot . . . . .  | 8  |
| 2.6   | WL-9DR walking robot . . . . .   | 8  |
| 2.7   | P3 model on the left and ASIMO on the right . . . . .                    | 9  |
| 2.8   | HPR-2 humanoid robot . . . . .   | 9  |
| 2.9   | A prototype of a single DOF biped robot at LARM . . . . .                | 10 |
| 2.10  | Pasibot Robot . . . . .  | 10 |
| 3.1.1 | Hoeken straight-line linkage . . . . .                                   | 11 |
| 3.2.1 | Pantograph . . . . .   | 12 |
| 3.3.1 | Single leg mechanism . . . . .   | 13 |
| 3.5.1 | Parallel Extension . . . . .   | 15 |
| 3.6.1 | Single leg with parallel extension . . . . .                             | 16 |
| 4.1   | Single leg mechanism . . . . .   | 18 |
| 4.1.1 | Denavit-Hartenberg kinematic parameters . . . . .                        | 19 |
| 4.2.1 | Frames' position and orientation Hoeken's Linkage . . . . .              | 20 |
| 4.2.2 | Frames' position and orientation pantograph . . . . .                    | 20 |
| 4.2.3 | Closed Loops . . . . .   | 21 |
| 4.2.4 | Comparison between two different gait pattern . . . . .                  | 23 |
| 4.2.5 | Gait pattern of two-legged walking robot . . . . .                       | 24 |
| 4.2.6 | Gait pattern considering toe as end effector . . . . .                   | 25 |
| 4.2.7 | Body posture with punctiform foot . . . . .                              | 28 |
| 4.2.8 | Body posture with foot of fixed length . . . . .                         | 29 |
| 4.3.1 | Frame's first loop . . . . .   | 30 |
| 4.3.2 | Frame's second loop . . . . .  | 30 |
| 4.3.3 | Frame's third loop . . . . .   | 31 |
| 4.3.4 | Closed loop leg mechanism with parallel extension . . . . .              | 32 |
| 4.3.5 | Gait pattern of toe using parallel extension . . . . .                   | 33 |
| 4.3.6 | Body posture with parallel extension . . . . .                           | 34 |
| 5.1   | Linear velocity and acceleration of end effector (ankle joint) . . . . . | 36 |
| 6.1.1 | Prototype of walking robot in Inventor Pro 2020 . . . . .                | 37 |
| 6.2.1 | Path of ankle and toe . . . . .  | 38 |
| 6.3.1 | Linear velocity of ankle . . . . .                                       | 38 |
| 6.3.2 | Linear acceleration of ankle . . . . .                                   | 39 |
| 7.1.1 | Mass distribution and center of mass of links . . . . .                  | 40 |
| 7.2.1 | Torsion Spring . . . . .   | 42 |
| 7.3.1 | Examples of free body diagram . . . . .                                  | 43 |
| 7.3.2 | Torques . . . . .  | 44 |
| 7.3.3 | Twist angle $\Delta\beta$ . . . . .                                      | 45 |
| 7.4.1 | First Simulation . . . . .   | 46 |
| 7.4.2 | Second Simulation . . . . .  | 47 |
| 7.4.3 | Third Simulation . . . . .   | 48 |
| 7.4.4 | Fourth Simulation . . . . .  | 49 |



## List of Tables

|   |    |
|---|----|
| 3.1.1 Lenght of Hoeken's links . . . . .  | 11 |
| 3.2.1 Lenght of pantograph's links . . . . .  | 12 |
| 3.3.1 Length of Links . . . . .   | 14 |
| 3.5.1 Length of links Parallel Extension . . . . .  | 15 |
| 3.6.1 Length of Links . . . . .   | 17 |
| 4.2.1 First closed chain . . . . .  | 21 |
| 4.2.2 Second closed chain . . . . .   | 22 |
| 4.2.3 Third closed chain . . . . .  | 22 |
| 4.2.4 Denavit-Hartenberg table with foot . . . . .  | 26 |
| 4.3.1 Denavit-Hartenberg table for first branch (0-1-4-10) . . . . .                      | 30 |
| 4.3.2 Denavit-Hartenberg table for second branch (0- $\tilde{10}$ -10) . . . . .          | 30 |
| 4.3.3 Denavit-Hartenberg table for first branch (0-1-4-9-11) . . . . .                    | 30 |
| 4.3.4 Denavit-Hartenberg table for second branch (0-1-4-6- $\tilde{11}$ ) . . . . .       | 30 |
| 4.3.5 Denavit-Hartenberg table for first branch (0-1-4-6-13) . . . . .                    | 31 |
| 4.3.6 Denavit-Hartenberg table for second branch (0-1-4-9-11-12- $\tilde{13}$ ) . . . . . | 31 |
| 7.1.1 Mass distribution of human body . . . . .   | 41 |
| 7.1.2 Mass distribution of walking robot . . . . .  | 41 |